TÉCNICO LISBOA

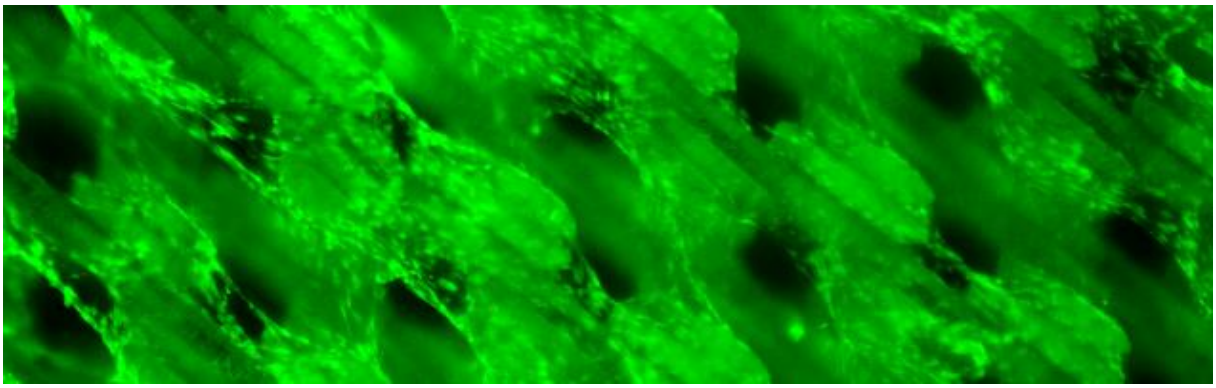

Mechanical properties of PTMC scaffolds constructed by Stereolithography for the repair of Annulus Fibrosus tissue. Effect of scaffold characteristics on cell adhesion and proliferation.

Ana Luísa Parruca da Cruz

Thesis to obtain the Master of Science Degree in

Biological Engineering

Supervisors: Dr. André A. Poot

Dr. Frederico Castelo Alves Ferreira

Examination Committee

Chairperson: Prof. Arsénio do Carmo Sales Mendes Fialho

Supervisor: Dr. Frederico Castelo Alves Ferreira

Members of the Committee: Dr. Carlos André Vitorino Rodrigues

October 2014

ACKNOWLEDGEMENTS

First of all I would like to express my gratitude to MIRA's BST group, and more specifically André A. Poot and Sébastien B. G. Blanquer, thank you for the opportunity to join this project and support. I would also like to acknowledge Sébastien B. G. Blanquer for constructing the scaffolds required for this study. To Lydia Versteeg-Bolhuis, thank you very much for teaching and accompanying me in this project, for the insights, advices and friendship.

Furthermore I want to thank my home institution, Instituto Superior Técnico, for the opportunities and training provided, but also for showing me the reality that nothing in this world comes without confidence, hard work and resilience.

To everyone throughout my life, thank you for the bad times that taught me to never give up and more importantly, gave me the ability to overcome whatever comes in my way. Thank you for good memories, those I will always treasure.

Mom and dad: part of this is yours, thank you for raising me the way you did.

Grandparents: you showed me that is good to be smart and intelligent, but better to be wise and share your wisdom

Brother: for setting goals to overcome

Uncles and Cousins: for always being present and for being a reminder that is good to be young

Carolina and Joana: by listening to my insanities you kept me sane for the past 5 years and became like family to me

Tiago: living prove that the best in this world comes with work but also love, patience and genuine care

"*Haja ou não haja frutos, pelo sonho é que vamos"*

Sebastião da Gama

I ABSTRACT

Degeneration of the intervertebral disc affects around 97*%* of individuals 50 years or older in a worldwide scale and is known to prompt cases of chronic low back pain as well as some related pathologies, such as disc herniation. Current treatment options are costly, invasive and relatively ineffective, being solely based on pain management and lacking capability of rehabilitation of the bio-mechanical characteristics of disc structure. Furthermore outcomes are limited regarding disc functionality and can lead to further degeneration. As an alternative, tissue engineering strategies are being developed in hope to regain total disc functionality. Regeneration of the outer layer of the disc, the *annulus fibrosus*, is the most challenging because of its complex organization. In the current project we optimize the design characteristics of a previously developed gyroid architecture Poly-(trimethylene carbonate) scaffold built by stereolithography for repair of the AF tissue. Scaffolds seeded with human *annulus fibrosus* cells displayed excellent cell adhesion and distribution. Higher rates of proliferation were observed for higher pore sizes (493 *µm*) and porosities (≥ 67 *%*). Scaffolds with a pore size of 400 *µm* and 70 *%* porosity, exhibited an increase of two times their initial value of compression *modulus*, after 14 days of culture, reaching a value of 0.609±0.215 *MPa* comparable to that of native human AF tissue. PTMC built scaffolds exhibit promising bio-mechanical properties, increasing its relevance when constructing functional AF replacements.

Key words: Intervertebral Disc; Disc Degeneration; *annulus fibrosus* Regeneration; Bio-mechanical characteristics; Poly-(trimethylene carbonate); Scaffold Design

II RESUMO

A degeneração do disco vertebral afeta a nível mundial cerca de 97 % da população com 50 anos ou mais, sendo precursora de lombalgias crónicas. Os tratamentos atualmente disponíveis são caros, invasivos e relativamente ineficientes, uma vez que se limitam a gerir a dor do paciente, negligenciando a reabilitação das características biomecânicas do disco. Além disso, levam muitas vezes a uma recorrência do processo de degeneração do disco ou de discos adjacentes. Têm sido desenvolvidas no âmbito de engenharia de tecidos, alternativas com o objetivo de recuperar as funcionalidades do disco. Devido à sua complexidade, reparação da parte exterior do disco, o a*nnulus fibrosus*, é especialmente desafiante. No presente estudo otimizámos as características de projecto de uma matriz de suporte de proliferação de células para reparação do *annulus fibrosus*. Matrizes com uma arquitetura giróide foram construídas por recurso a estereolitografia por *foto-reticulação* do polímero sintético Poli-(Trimetileno Carbonato). Células humanas do a*nnulus fibrosus* foram cultivadas, mostrando boa adesão e distribuição nas matrizes. Maiores taxas de proliferação foram obtidas para matrizes poliméricas com maior tamanho de poro (493 μm) e porosidades (≥ 67 *%*). Analisando as propriedades mecânicas, matrizes com poros de 400 μm apresentaram um aumento de duas vezes o seu valor inicial de módulo de compressão, depois de 14 dias de cultura, atingindo um valor de 0.609±0.215 *MPa*, comparável aos valores bibliográficos obtidos para o tecido nativo. Matrizes porosas construídas com PTMC exibem propriedades biomecânicas promissoras na construção de uma solução funcional para reparação do *annulus fibrosus*.

Palavras-Chave: Disco Vertebral; Degeneração do Disco; Regeneração do *annulus fibrosus*; Propriedades Biomecânicas; Poly-(trimetileno Carbonato); Projecto de Matrizes de Proliferação de Células

III TABLE OF CONTENTS

IV LIST OF TABLES

V LIST OF FIGURES

VI LIST OF ABBREVIATIONS

$	American Dollar
°	Arc Degree
°C	Celsius Degrees
2D	Two Dimensions
3D	Three Dimensions
AF	Annulus Fibrosus
AFC	Annulus Fibrosus Cells
BMG	Bone Matrix Gelatin
BST	Biomaterials Science and Technology
C	Constant Value for Scaffold Design
CAD	Computer Aided Design
CEP	Cartilaginous Endplate
CFR	Relative Centrifugal Force
CT-scanning	Computer Tomography Scanning
E	Young's or Elastic/Tensile *Modulus* (*MPa*)
ECM	Extracellular Matrix
FBS	Fetal Bovine Serum
GAG	Glycosaminoglycan
G_{eq}	Shear *Modulus* (*kPa*)
GFP	Green Fluorescent Protein
H_A	Aggregate *Modulus* (*MPa*)
hAFC	Human Annulus Fibrosus Cells
HNP	Herniated Nucleus Pulposus
Hz	Hertz
IDD	Intervertebral Disc degeneration
IVD	Intervertebral Disc
kg	Kilogram
L	Litre
l	Length
LBP	Low Back Pain
LFH	Laminar Flow Hood
LMBS	Loffler's Methylene Blue Solution
m	Meter
MB	Methylene Blue
MIS	Minimal Invasive Surgeries

M_n	Average Molar Mass (*g/mol*)
mol	Amount of Substance
MSCs	Mesenchymal Stem Cells
n	Number of Samples
N	Newton
NP	Nucleus Pulposus
NPCGS	Nucleus Pulposus cell Growth Supplement
NPCM	Nucleus Pulposus Cell Medium
nr	Identification Number of the Scaffold
P	Probability
P/S	Penicilin / Streptomycin Solution
Pa	Pascal
PBS	Phosphate Buffer Solution
PCD	Programed Cell Death
PCL	Poly(Ɛ-caprolactone)
PCU	Polycarbonate Urethane
PDLLA	Poly-DL-Lactide
PEO	Poly-(Ethylene Oxide)
PFA	Paraformaldehyde
PG	Proteoglycan
PGS	Proteoglycans
PPCLM	Polycapro- lactone Triol Malate
PTMC	Poly-(trimethylene Carbonate)
PU	Polycarbonate Urethane
R^2	Correlation Coefficient
ROS	Reactive Oxygen Species
rpm	Rotations Per Minute
SD	Standard Deviation
SFF	Solid Free Form
SL	Stereolithography
TGFβ-1	Transforming Growth Factor Beta 1
TMC	Trimethylene Carbonate
TMP	Tri(hydroxymethyl) Propane
TXRed	Texas Red
US	United States
W	Watt

1. INTRODUCTION

1.1 THE INTERVERTEBRAL DISC

The intervertebral disc (IVD) is a complex structure formed by a semi-cartilaginous tissue, located in the vertebral column between the cartilage endplates of the column's vertebrae [(1)] (Figure 1:1). The human spinal column is composed by 23 intervertebral discs, each one with an average 4 *cm* in diameter and 8 to 10 *mm* in height [(2)].

Although being composed by different, but related tissues, with varied properties, the whole IVD is in fact responsible for joining the several vertebrae, movements like flexion and torsion of the spine, and also the bearing of loads and forces of impact [(2), (3)]. The IVD can be differentiated into two different anatomical zones, the *nucleus pulposus* (NP) and the *annulus fibrosus* (AF) [(1), (4)], these have different functionalities, cell populations and extracellular components (ECM). The intervertebral disc's ECM is an extremely complex entity and has a key role on the mechanical and chemical properties of the disc as well as a strong influence on cell migration, proliferation and behaviour.

The IVD is the largest avascular organ in the human body, thus a gradient of metabolites and nutrients is formed between the peripheries of the disc and its center [(3)]. This fact also has an effect on the environment of the disc, making it a low oxygen and a low pH tissue (about 6,9 to 7,1 *pH*), when compared to the common levels of blood plasma [(3)]. Nutrition of the disc is mainly made through the adjacent vertebral bodies in the endplate pathway and also by the AF pathway. The metabolism of the cells present in the IVD is mainly anaerobic, with production of lactic acid as a result of cellular activity [(2), (5)].

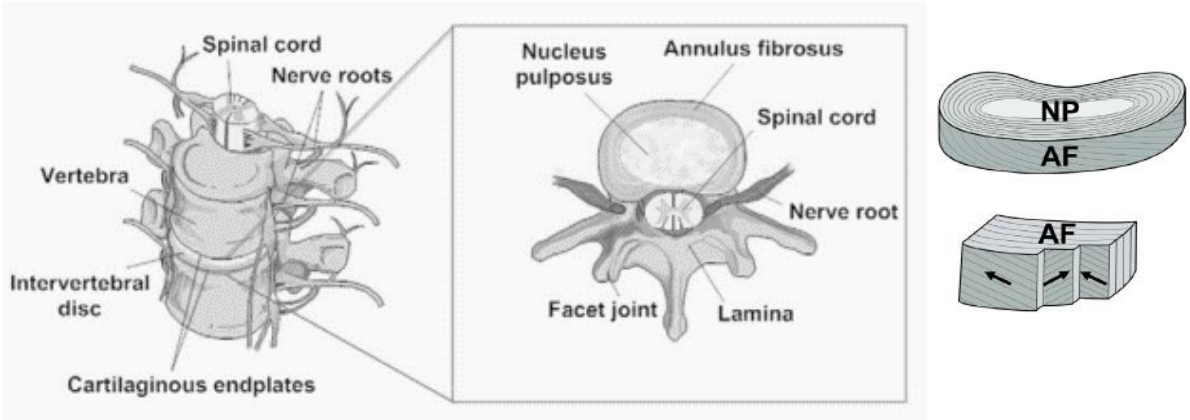

Figure 1:1 Left image: Illustration of a healthy intervertebral disc. Representation of the disc positioning between the vertebrae and overall structure of the IVD (Source: Joana Silva-Correia *et al* 2010 [(2)]); Right Image: Concentring lamella of the *annulus fibrosus* with alternating collagen fibres alignment (Source: Martin *et al* 2014 [(6)]).

1.1.1 Nucleus Pulposus

The *nucleus pulposus* is the core of the IVD and is composed by a highly hydrated [2], [1], gelatinous and homogeneous mass. Its high fluid and proteoglycan (PG) content allows it to maintain the high osmotic and interstitial fluid pressures. Other extracellular components that also contribute for NP microenvironment are collagen type II and a small amount of elastin that supports the proteoglycan network, mainly composed by aggrecan. By its turn, aggrecan is responsible for linking highly sulphated glycosaminoglycans (GAGs) that maintain the NP hydrated [2]. The NP has a viscoelastic behaviour that allows its structure to expand under compressive forces, radially distributing the forces in an isotropic manner [1], [7]. Nevertheless the NP is very sensitive to environmental changes [8], [9] and cells present low mitotic and regeneration capabilities, as it will be addressed later on the section 1.2 regarding disc-related pathologies.

The cells that populate the *nucleus* pulposus are rounded, being comparable to chondrocytes and producing ECM similar to that present in hyaline cartilage. Despite a consensus has not been reached between researchers, studies suggest that the NP cells are originally derived from the notochordal cells. However, since in humans with increasing age the concentration of notochordal cells diminishes, some researchers believe that the NP structure is populated with cells similar to chondrocytes, that result from the migration of cells from adjacent tissues like the inner AF or the cartilaginous endplates [2] [7]. Recent studies also revealed the presence of cells with mesenchymal stem cells markers in the healthy and degenerated IVD [2].

1.1.2 Annulus Fibrousus

Surrounding the *nucleus pulposus* is the *annulus fibrosus*, a lamellar and fibrocartilaginous structure, which is built to resist large and compound loads that arise during physiologic joint movements [7]. The AF is anchored to the endplates and connected to the vertebral bodies by “Sharpey’s fibers” that hold the IVD structure in place. Besides the previously mentioned functions, the AF also prevents the NP from leaking [3].

The AF structure is more dense than the NP but less hydrated [2], [10], representing about 65 to 90 *%* of the IVD’s dry weight [10]. The several concentric lamellae that compose the AF (15 to 25 *maximum*) are composed by highly oriented and organized collagen fibbers, mainly type I, that represent in average 60 *%* of the dry weight of the whole disc [10] [11]. These are inserted in a non-fibrilar hydrated network of proteoglycans [11], being separated by the interlamellar *septae* that are a mixture of linking elements and a proteoglycan matrix [10]. Elastin fibres are interlaced among the collagen, permitting the disc to go back to its initial location after movement [10].

Because they exhibit markers of both fibroblasts and chondrocytes, the AF cells are considered fibrochondrocytes [2], [11]. These are present in a density two times higher than in the NP tissue, about $9 \cdot 10^6$ *cells/cm*^{3} in mature healthy subjects [10], [3]. Recent studies conducted by Jin *et al* in 2014 support the hypothesis that AF cells can behave like progenitor cells, being able to differentiate into osteoblasts and chondrocytes under suitable culture conditions and stimuli [12]. However it is not known if this ability emerges from a process of differentiation or dedifferentiation of the cells.

According to the structural and cellular variances, the AF tissue can be further separated in inner AF and outer AF. In fact even the mechanical load that each part of the AF sustains is different, the inner AF for being

closer to the NP is subjected to greater hydrostatic pressures, and the outer AF bears higher tensile forces [10]. This differences will also influence the extracellular matrix (ECM) production and turnover, contributing to the formation of gradients [10]. In the outer AF the collagen fibres are distributed in what is called an angle-phy organization, meaning that besides following the circular organization of the disc, the fibres present opposing directions in each lamellae [8] [11].

Because of its proximity to the NP, the inner part of the AF consists in a mixture of the extracellular matrix of the mentioned tissue [10], also the cells of this part of the AF present a chondrocyte-like behaviour and tend to be round and sparse as opposed to the cells of the outer part of the AF, that behave like fibroblasts, being ellipsoidal with long axes that and aligned with the collagen fibres [13]. It was also observed that in the inner AF the lamellae are more spread from each other than in the outer AF. The most common ECM components of the *annulus fibrosus* are synthesized in annex 7.2.1.

1.1.3 Mechanical Loading

Due to the verified differences between the positioning and extracellular matrix and cell composition of the several structures of the intervertebral disc, each experiences different types of stresses, from compression to bending, flexion, extension and torsion [14]. This results in multidirectional loadings and deformation of the IVD structure [15]. Cell type and ECM production have an anisotropic behaviour throughout the disc, as well as disc mechanical properties, which means that they change with the direction, however this mechanisms and differences are not fully understood yet [14], [15].

As mentioned before the inner AF is more exposed to the forces that emerge from the *nucleus pulposus*, being subjected to the radial compression and stress from the NP's fluid pressure [16], [17]. These are then converted into tensile forces on the collagen I fibres that compose the lamellae of the inner AF. The lamellas of the outer AF are essential to prevent AF tearing, once they allow the bending and torsion of the spine [17]. These movements cause circumferential tension and shear on the outer AF structure, which are mainly sustained by the stretching of the collagen fibres present at higher densities in this tissue [15]. Differences between the tissues are notorious, as an example the elastic *modulus* increases 65 times from the outer to the inner AF [16].

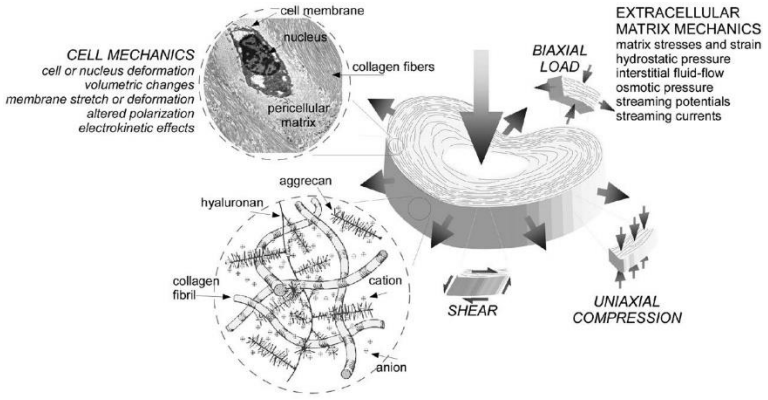

Figure 1:2: Different types of mechanical loading sustain by the disc. Large arrow: axial compressive loading, induces shearing and tensile stresses that are distributed to extracellular matrix, as well as an interstitial fluid phase that experiences changes in hydrostatic pressure (Source: Setton *et al* 2006) [7].

1.2 DISC DEGENERATION AND RELATED PATHOLOGIES

The normal production of extracellular matrix is essential for a healthy IVD, this is ensured by fibro-chondrocytic cells existing in this structure. When the production of ECM is altered by means of either degeneration or aging of the IVD tissue, the amount of extracellular matrix produced diminishes. In these cases, the decreased proteoglycan and type II collagen concentration results in loss of disc height and hydration of the NP tissue, as seen in Figure 1:3, putting more pressure on the fibres of the AF, which can tear, thus enabling the leakage of NP, forming an hernia [8], [3]. Nevertheless, disc herniation and other pathologies can also be caused by traumatic events where damaging forces are applied or by inflammation of the IVD structure [2], which lead as well to the degeneration of the IVD. Cases of disc protrusion can also be observed, this is a condition predecessor to herniation in which the outer layers of the AF remain intact, but can bulge when the disc is under pressure. In protrusion cases there is no escape of NP tissue.

Some researchers propose that disc degeneration and herniation are somehow related to some unknown genetic factors [2]. A study conducted by Kepler *et al* early in 2013 suggests that 75 % of the initial susceptibility to disc degeneration is due to genetic factors, being environmental factors less predominant [18]. When the intervertebral disc starts to degenerate, major alterations are observed and the biochemical balance of the disc is lost. Cells stop to divide in a phenomenon called cell senescence, there is an increase in the production of matrix-degrading enzymes and collagen, decrease of pH and oxygen levels, increased expression of proinflammatory cytokines and a raise in the rates of programmed cell death (PCD or apoptosis), among others [18] [2]. Progressive structural alterations are also present on degenerated discs, the initially demarcated anatomical zones of the disc (NP and AF) become less evident, there is a reduction of the disc's thickness and a loss of AF fibres orientation [8] [2] (Figure 1:3).

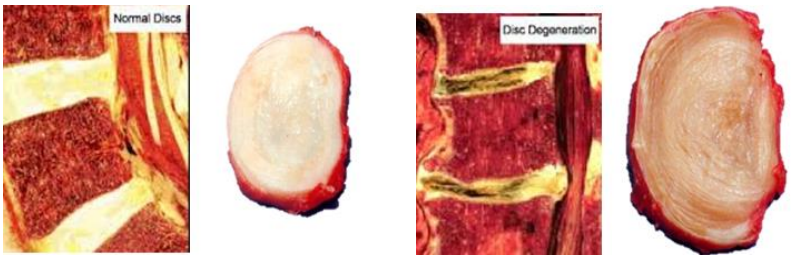

Figure 1:3 Differences between a heathy intervertebral human disc (on the left) and a degenerated disc (on the right): loss of disc weight and density. (Source: cross-section images SpinaStenosis.org [19], top-view images: Spine Bioengineering Laboratory [20])

Low back pain (LBP) is associated with several spinal pathologies [2], and its occurrence varies from person to person, according to the subject's age, general health, bone mass index, strength of the abdominal and back muscles and some day-to-day habits such as smoking or the bearing of heavy loads [2], [21]. The mentioned factors may decrease the availability of blood in the tissue, so it is more difficult to supply nutrients to the cells and consequently they lose part of their activity and viability [2], progressing or initiating the degeneration process

[21]. The increased age and degeneration of the IVD causes the accumulation of high concentrations of toxic metabolites, within which it is important to highlight the raise of lactic acid levels, which lowers the pH, hence modifying ECM production and preservation [2]. Also, there is an increased production of reactive oxygen species (ROS) that can be responsible for the induction of the apoptosis mechanisms in the NP cells [2, 22]. Low back pain is usually the main symptom of disc degeneration, but is mostly presented in advanced stages of the degeneration, when the AF is affected but in which the whole IVD structure, including cartilage endplates and NP are already altered. This happens because the IVD structure has few pain receptors that are mainly present at the margins of the disc [2].

About 45% of the cases of LBP are associated with a discogenic cause, which may derive from damage to more than only one IVD [23]. Discogenic LBP is provoked either from fissures and tearing of the AF or from focal defects of the outer AF [8]. Because of its low blood supply and small number of cells, the AF tissue has low capability to regenerate itself, so the healing process is usually characterized by the production of new connective tissue, called granular tissue, complemented with neovascularization, ingrowth of nerve fibres [8] and sometimes ingrowth of bony outgrowths [2]. This way, there is a creation of a state of chronic low back pain, in cases without herniation of the disc [2]. In the case of disc protrusions or herniation, LBP results as a mixture of nerve root ischemia and inflammation of the tissues near the extrusion [8]. In addition to local pain, when the disc is herniated (Figure 1:4) it may compress the segmental nerves, which by itself creates irritation and inflammation of the nerves. Ultimately this can lead to loss of function of the nerves and spreading of pain [2].

Aforementioned the degeneration process deteriorates the whole disc structure, so many other spinal diseases may progress from this condition including bone and soft tissue pathologies, besides the ones mentioned before, some examples are internal disc derangement, lumbosacral radiculopathy, and spinal canal stenosis [21].

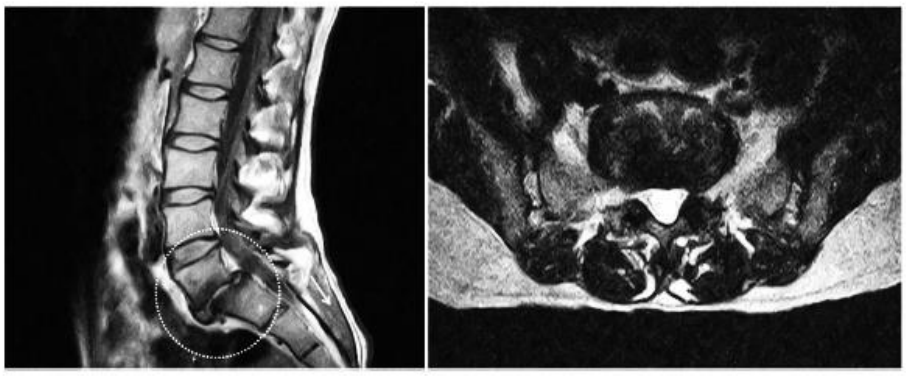

Figure 1:4 MRI image of a 40-year-old female's patient herniated intervertebral disc (Source: Joana Silva-Correia *et al* 2010) [2].

Disc Degeneration has a detrimental impact in several bio-mechanical properties of the disc, gradually reducing its capacity to normally function (Table 1:1). According to Kirkaldy-Willis's hypothesis, in early stages of degeneration the disc presents hypermobility and increased flexibility, which easily leads to stiffening of the tissue that becomes hypomobile, with associated pain [8] [20]. The nucleus pulposus is the most affected structure in the degeneration process, with loss of pressurization and support of larger loads, these are reflected in a decrease on the swelling pressure, relative energy dissipation and an increase of the shear *modulus*. Aforementioned, in the degeneration process of the AF tissue, there is also a loss of the water content accompanied with tissue compaction which leads to an increase on the compressive *modulus* and decreased radial permeability. [20]

Table 1:1 Mechanical and physical properties of a healthy and degenerative disc (Source: Guterl *et al* 2013 [8]).

	Property	Disc Grade	Property range
Organ Level / Motion Segment (*in situ* testing)	Disc height	Healthy	11.1±2.5 mm 11.3±0.3 mm
		Degenerative	9.2±2.9 mm
	Intradiscal pressure	Healthy	0.5 MPa (leakage pressure) 1.9 MPa (300 N load pressure)
		Degenerative	0.2 MPa (leakage pressure) 1.3 MPa (300 N load pressure)
	Torsional mechanics	Healthy	0.7°-0.8° (with 8° pelvic rotation) 3° max axial rotation
		Degenerative	1.8°-3.2° with 8° pelvic rotation
Tissue Level (*in vitro* testing)	H_A Compressive (confined compression)	Healthy	0.56±0.21 MPa
		Degenerative	1.10±0.53 MPa
	E Tensile (circumferential samples)	Healthy	12.7 MPa
		Degenerative	9.4 MPa
	Shear	Healthy	25<Geq (kPa)<110
		Degenerative	25<Geq (kPa)<140

1.2.1 Current treatment Options

At the present time, a great variety of treatment options for disc degeneration and related conditions are available. Nevertheless, these are more focussed on mitigating the symptoms, like for example low back pain, than treating the source of the pain. In most cases, conservative treatments are applied to control the patient's pain by resorting to pain killers, physical therapy and epidural steroid injections, if the condition is not manageable surgical procedures are considered [8], [2]. Several strategies have been developed for each step of the degeneration process. On first stages of degeneration cell, gene and even pharmaceutical therapies may control further disc degeneration and reduce the inflammation [6], [24], [25], see Annex 7.2.2.

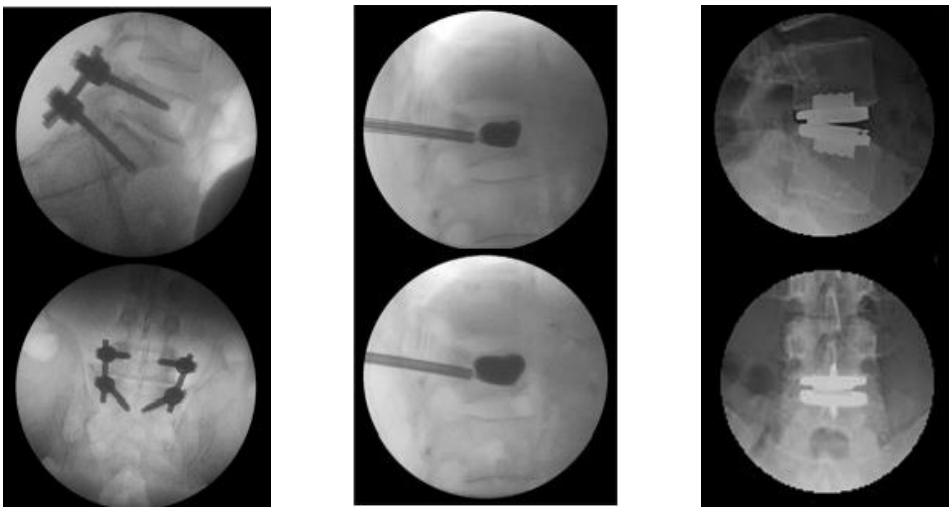

Figure 1:5 Common surgical procedures used for treatment of disc related pathologies. From the left to the right, lumbar fusion [2], vertebroplasty [2] and disc arthroplasty [26].

In terms of surgical procedures the treatments range from lumbar discectomy and/or spinal fusion, disc arthroplasty and dynamic stabilization, as displayed in Figure 1:5, to some minimal invasive methodologies. In the cases of LBP, discectomy is the most performed surgery in the USA [8], in this technique the degenerated disc is removed and the two adjacent vertebrae are fused together using a bone graft that is usually taken from the pelvic bone of the patient or from a compatible donor. This technique is effective in regard to the neurological symptoms [8], but has several disadvantages, like the reduction of the patient's column flexibility, recurrent herniation and the decrease of 25 % of the disc height that is associated with amplified and persisting LBP and disability [8] . It also causes increase stress to the adjacent vertebrae, that this way are more likely to degenerate [8] [2].

In cases of protrusion or minimal disc degeneration, discectomy is not the most favourable treatment option since it is quite drastic, in this cases the protruded tissue is removed in a small surgery instead. Although less aggressive, there is a high risk of recurrence of herniation and follow-up surgery is frequently needed [8].

Since low back pain and the majority of the complications that follow surgeries are mainly related to the AF structure, studies have been made on strategies to close the AF tissue. The most direct option is suture but this procedure is extremely challenging due to the small scale of the wounds, the lack of space and the high potential

to damage the adjacent neurological structures [8]. Although suturing proved to enhance the healing, it is not very significant. To close larger tears (> 3 *mm*), that result from surgeries where the herniated tissue is removed or where the inner AF is affected, some implants are already available like InClose®, that seals and sutures the AF or Barricade® ,that anchors the AF to the near bone [8]. Although promising, these implants still have not been proven to be efficient and applicable to numerous types of defects, comprehending risks of dislocation of the implant [8]. In more recent studies, researchers attempted to use fibrin and/or cyanoacrylate based glues in combination to traditional suture, to achieve AF closure and although some improvements were observed, additional optimization of the procedure is still necessary [2].

Low back pain and disc degeneration have a massive detrimental impact on modern's society, from a social, economic and medical point of view [2]. It normally affects the working [10] and the elderly population [2], with high associated costs regarding the treatment procedures, for example just in the USA, medical and absence related costs reach US$100 bilion [27]. Also, for the treatment of low back pain, which as a high lifetime prevalence situated between 58 *%* and 84 *%* [2], patients commonly require extended times of bed rest and hospitalization, which leads to an increase of work absenteeism.

Since the population as currently has a tendency for aging, at a worldwide scale, a raise in the incidence of intervertebral disc degeneration and low back pain cases is expected [3]. All these factors make it increasingly important to find a solution that can provide a better outcome for the patients and that significantly lowers the recurrence rates. This way, tissue engineering strategies are starting to emerge as an attractive alternative to conventional treatment options.

1.3 TISSUE ENGINEERING APPROACHES

In tissue engineered approaches cells isolated from the patient or from a compatible source are cultured and then seeded in a scaffold. The scaffolds, made of a specific biomaterial, usually have a tailored 3D shape, as well as chemical and physical properties that try to mimic those of the native tissue so that cells can easily proliferate with the wanted phenotype and spread throughout the scaffold. When the scaffold presents the desired biological and biomechanical characteristics, it is transplanted into the patient's body to induce regeneration of the damaged areas and/or generation of new tissue. In tissue engineering techniques, constructs can be implanted alone or associated with biologic active compounds, like growth factors, drugs, among others [(2), (28)]. The scaffold is usually biodegradable so that in early stages after grafting it can serve as a support structure for the cell and tissue development.

As mentioned before, the traditional treatment options available for conditions related to LBP are very limited and unsatisfactory, so tissue engineering techniques are evolving with the objective of developing a solution that not only diminishes the pain felt by the patient, but also restores the intrinsic properties of the disc [(2)] and enhances them, if possible. Tissue engineered solutions for IVD are primarily aimed at increasing the disc height and at re-establishing the majority of the biomechanical features, because only this way it is possible to promote regeneration that will enable the recovery of spine functions [(2)].

In the past decade, research has been focused on *nucleus pulposus* regeneration [(10)] and, although great advances have been made in this field, the closure of the surrounding *annulus fibrosus* tissue is still the main challenge [(21)], when considering either NP replacement or pathologies that compromise the AF. Only by treating the AF tissue is possible to decrease the risk of re-herniation and increase the potential of NP healing, since with regeneration of NP there is a rebuilding of the intradiscal pressure, that even in conditions of less stress can tear the weakened AF tissue [(1), (10)]. Whole organ tissue engineered strategies can also be considered but only on more drastic cases of severe disc degeneration [(3)] (Figure 1:6).

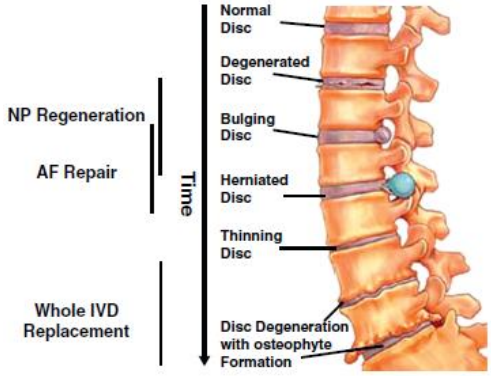

Figure 1:6 Progression of the degradation of the intervertebral disc with time, treatment options for the several conditions (Source: Silva-Correia *et al* 2013 [(2)]).

1.3.1 Tissue Engineering of the NP

As mentioned before, NP regeneration research is considerably more advanced than AF. The goal of this therapies is the replacement of the NP material that is usually lost in the degeneration process [3], this is made either by the injection of hydrated materials such as hydrogels, cells or/and molecules or the implantation of scaffolds [3], [29]. The most promising techniques rely on the use of hydrogels, such as methacrylated gellan gum and hyaluronan-derived hydrogels. Nevertheless the mechanical behaviour of the repaired NP still needs to be assessed, along with its performance and compatibility with tissue formation.

Although the NP is not the main focus of this study it is important to understand that this structure is closely related to that of AF. Furthermore, the success of NP therapies is dependent on a healthy AF and the AF repair is, in its turn, dependent on the capability of the NP to sustain shocks and carry loads. Also, one of the problems of injectable therapies applied *in vivo* is the damaging of the AF structure that can lead to tears and herniation.

1.3.2 Tissue Engineering of the AF

Several strategies have been considered to regenerate the AF structure and function, these involve cell therapy, gene therapy and tissue engineering [10]. However it was shown that by their own, cell and gene therapies are inefficient in the closure of the AF defect and do not prevent of further degeneration [10]. Nowadays, it is considered that the best treatment option involves the combination of cells with scaffolds and possibly other molecules, like growth factors.

When considering tissue engineering strategies for AF repair, it is important to have in consideration the complex AF structure, since repair of the AF tissue is only going to be efficient and successful if the regeneration process can re-establishment the structural, mechanical and biological properties and functions of the native tissue. Engineered AF has to support the fluid flow for the pressurization of the NP, stand the loads created by torsion and bending and provide a quick closure to the defect. These factors are essential to prevent further disc degeneration [8], [10]. Further challenges present in AF repair strategies include the non-uniform constitution of the ECM components and AF microstructure, which are hard to achieve.

To date, no tissue engineered solution as yet proved to be completely efficient in repairing the AF structure and reverse the degeneration process. Furthermore, to date there is no indication of clinical trials [2], nevertheless several studies are being conducted to improve the limited recovery outcomes of those who suffer from a degenerated disc or related pathologies [8].

1.4 SCAFFOLDS FOR AF TISSUE ENGINEERING: PREVIOUS RESEARCH

A wide range of construction methods, architectures and materials have been used in studies to construct a tissue engineered alternative for the AF structure (Figure 1:7). The scaffolds should be functional and help the regeneration process [2], acting not only as a physical support to cells but also promoting cell growth, proliferation and ECM production with its architecture. It must be degradable so that cells and ECM can slowly replace the scaffold's function and it should be biocompatible so that no adverse reactions are caused.

One of the first materials considered for tissue engineering of the AF were hydrogels. Different formulations, composed of collagen alginate, agarose and chitosan have been tested over the past years. Although these gels usually are very biocompatible, immunologically tolerated by the cells, and easy to apply in the defect, they are still lacking the needed mechanical properties for AF tissue engineering, not being able to sustain stress and shear in the AF. As an example, Guillaume *et al* developed early in 2014 a shape-memory porous alginate hydrogel by freeze-drying, this presented the advantage of direct biomaterial delivery to the damaged area in a minimal invasive approach, nonetheless, even after 21 days of culture the mechanical properties were still far from those of human AF tissue, due to immaturity of the deposed ECM [30]. More recently in 2014, an injectable fibrin-genipin adhesive hydrogel was produced to repair large AF defects. This hydrogel prevented disc height loss, maintained the viability of AF cells near the repair site and presented good mechanical properties, however tensile and torsional stiffness were not fully restored [31].

Furthermore, previous work demonstrated that some hydrogels, such as alginate or matrigel, change the phenotype of AF cells and with culture time these start to resemble NP cells [3]. In a recent work, Sheck and co-workers developed a crosslinked genipin-fibrin hydrogel with mechanical properties in the range of native AF tissue [2]. Although the results showed that the constructs were biocompatible with excellent adhesive properties, a low cell proliferation rate and rounded morphology of the cells was also observed. For these reasons, the authors concluded that this biomaterial was best suited as a sealant for small AF defects or as an adhesive to large AF repairs [2].

Electrospinning is a technique widely used for mimicking the native AF lamellar structure. In this technique, oriented micro or nanofibres are arranged in a way so that porous membranous structures are produced, resembling the size and the natural angles formed by the collagen fibres of the AF [6], [16], [32], [33], creating a microenvironment close to the one of the native tissue.

Several materials have been used from silk [1], [34] to alginate [2], collagen-hyaluran [2], collagen-fibrin [35], polycarbonate urethane (PU) [16], among many others [29]. Studies demonstrated that oriented AF fibres can replicate the structural hierarchy of the AF, promoting AF phenotype and contributing to enhance the mechanical stiffness of electrospun scaffolds, since there is an orientation of the cells and the deposited ECM [6]. However these are far from reaching those of native IVD. In an experiment conducted by Nadan L.Nerurkar *et al* in 2008 [11], poly(Ɛ-caprolactone) (*PCL*) nanofibrous scaffolds were constructed and seeded with bovine AF cells, demonstrating that organized and anisotropic deposed ECM improved the mechanical properties of the constructs, nonetheless, these exhibited low cell infiltration and distribution, a common drawback of electrospun

scaffolds [6], [11], [32], [36], [37]. Similar results were obtained by Martin *et al* in 2014 for electrospun *PCL* scaffolds [6], even though a layer of sacrificial poly(ethylene oxide) (PEO) was added to the construct to better cell infiltration.

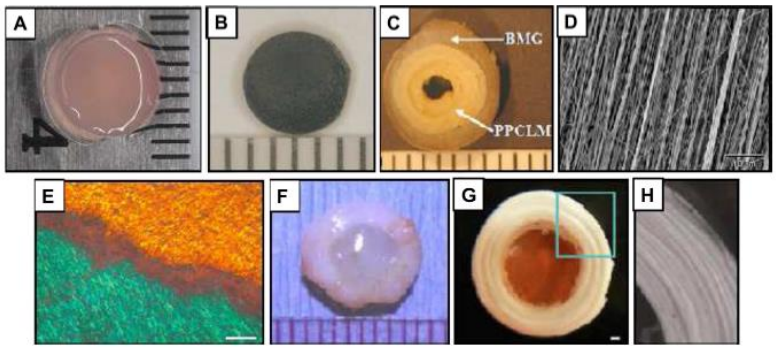

Figure 1:7 Previously used materials for tissue engineering of the AF and IVD structure. (Source: Iatridis *et al* 2013 [14]). (A) Photocross-linked carboxymethylcellulose hydrogel for NP;(B) Fibrin-genipin adhesive for AF fissures;(C) Biphasic scaffold: PPCLM surrounded by BMG (D) Electrospun polycarbonate polyurethane scaffold; (E) Electrospun PCL nanofibrous scaffold. (F) Alginate hydrogel surrounded by a poly(glycolic acid);(G) Disc-like angle-ply structure: PCL nanofibres and agarose hydrogel;(H) Magnified image of the AF region in the G panel. [14]

Some studies conducted to date used dynamic culture conditions with application of mechanical stimuli (torsion/ compression shear). These were proved numerous times to enhance the cellular metabolic activity and ECM deposition when compared to static culture [16], [34], [38]. These studies also give valid information about gene regulation and protein expression, some manifest increased collagen type I, elastin and *TGFβ-1* gene expression and increased GAG production with mechanical stimuli [16], [34]. However, further studies are required to determine optimal forces for correct tissue formation.

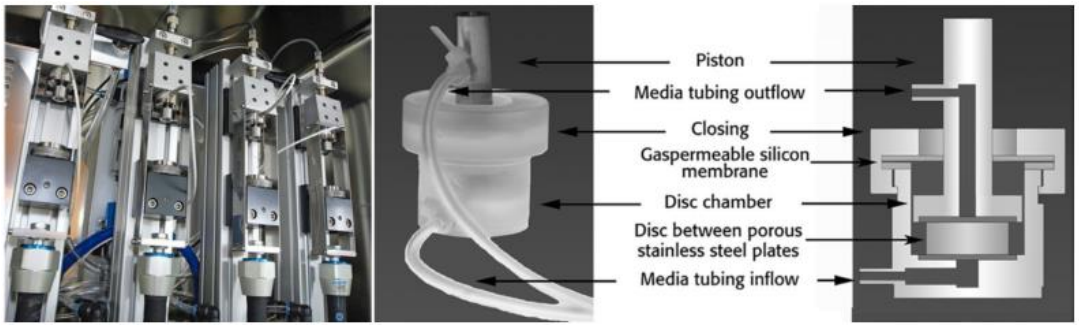

Figure 1:8 Bioreactors for culture of IVD constructs equipped with *mechanical stimuli* (Source: Guterl *et al* 2013 [8]).

More conventional methods were also used for producing porous scaffolds, like freeze-drying, salt leaching and phase-separation, nevertheless, these techniques do not produce a replicable structure, being almost impossible to achieve a limited and defined pore network [39]. New techniques of rapid prototyping like stereolithography started to emerge and develop more recently, allowing a controlled and fast fabrication of scaffolding structures.

1.5 RESEARCH PROJECT

1.5.1 Aim of Study

This study aims to optimize the design parameters of a PTMC stereolithography built scaffold for *annulus fibrosus* tissue repair.

1.5.2 Research Strategy

When building a scaffold for tissue engineering, every aspect from scaffold's material and architecture to cell source is relevant for the biological and mechanical properties of the construct, once these will determine the success or failure of the same. Previously we mentioned different scaffolds and materials that have been recently constructed for application in AF tissue engineering, nevertheless, they all show some limitations and disadvantages.

Application of solid freeform fabrication techniques is relatively new in the field of AF tissue engineering, but has presented good outcomes in previous studies [40], [4], [41]. In the current project we hope to optimize the design parameters of a PTMC scaffold built using stereolithography, constructed with a gyroid architecture and seeded with human *annulus fibrosus* cells (hAFC). Moreover, we intend to assess the effect of culture time (24 hours, 7 days and 14 days) on the mechanical properties of the porous scaffolds by means of compression tests and compare to those of native tissue, wet and dry PTMC constructs previously studied [40].

Design parameters are not independent of each other, so different experiments of constant surface area and constant pore size were performed to assess the effect of pore size and porosity, respectively. Cell adhesion, proliferation and distribution were investigated performing a Methylene Blue staining after 24 hours, 7 days and 14 days of culture. Cell Viability was assessed using a Live/Dead assay.

1.5.3 Research System Components

1.5.3.1 Stereolithography

Stereolithography is a sort of solid freeform fabrication (SFF) technique, first presented in 1986 that uses as principle photo-polymerisation [28]. Although not very recent, this technique is always evolving and continues to be frequently used, since it allows the creation of high quality scaffolds with really complex structures that can be created directly from scanning data from imaging techniques like MRI images, mathematical equations or from computer aided designs (CAD) [28], [42].

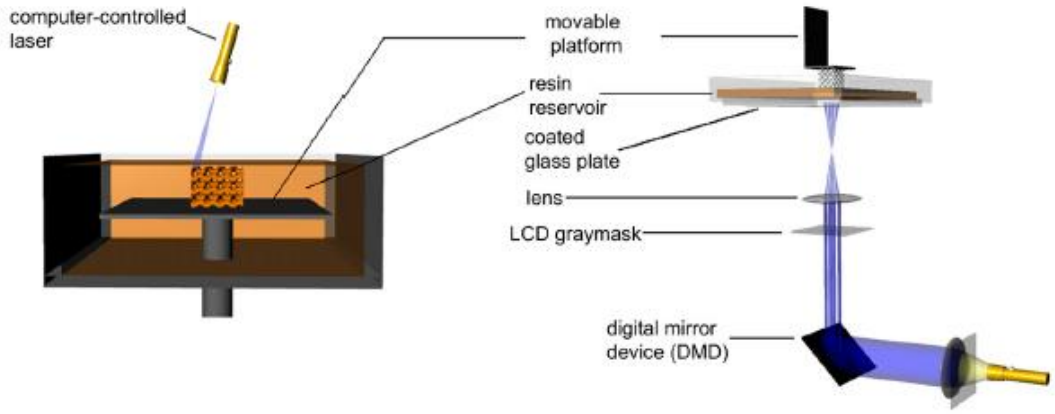

Figure 1:9 Illustrations of stereolithography set-ups. On the left: computer-controlled laser system (bottom-up construction), on the right: Digital light device (top-down construction). (Source: Mechels *et al* 2010 [28])

Stereolithography (SL) is a very accurate and high resolution technique that is easily adapted to produce several predetermined scaffold architectures, allowing reasonable variations of scale (from *μm* to *cm*). It used to be limited to the quantity of available materials that could be used, but now the number of polymers compatible with this technique is increasing, and the associated costs are diminishing [28]. Nowadays, most of the resins used in stereolithography are based on functionalized poly[(D,l-lactide)-co-(Ɛ-caprolactone)] or poly(trimethylene carbonate) macromers [43]. The present study focused on the PTMC macromer, a photo-polymerizable and photo-crosslinkable polymer of high interest because of its elastic properties, which can be easily used in stereolithography [40], [4], [22] [43].

The SL is based on the partially controlled solidification of a photo-crosslinking liquid resin. Using adequate software, the *3D* design is transformed into *2D* slices that are then used as a base for the stereolithography machine to produce each layer. The laser, responsible for the polymerisation and solidification of the resin to a defined depth, is controlled by a computer so that it only irradiates specific parts of the resin's surface, according to the defined *2D* design. As the first layer is formed after photo-polymerization of a thin layer of the polymer, the resin adheres to a platform that then moves away from the surface so that a second layer can be cured. This way a complete *3D* scaffold is constructed in a layer-by-layer manner. Since the cure reaches a higher depth than the movement of the platform, connection between each layers is achieved [28]. The thickness of each layer is controlled by adjusting diverse parameters such as intensity of the light source, scanning time (laser systems) and explosion time to the light in projection systems [28]. After fabrication, the excess of the resin is drained and washed of the scaffold.

In terms of accuracy and resolution, stereolithography is better that other SFF techniques, but the resolution of the constructs is still extremely dependent on the size of the scaffold itself, so most of the SL machines are able to produce constructs that can reach some cubic centimetres in size, maintaining a good accuracy (≃20 *μm*). The accuracy is assessed comparing the initial computer design to the scan of the scaffold using computer tomography scanning (CT-scanning) [28] (Figure 1:10).

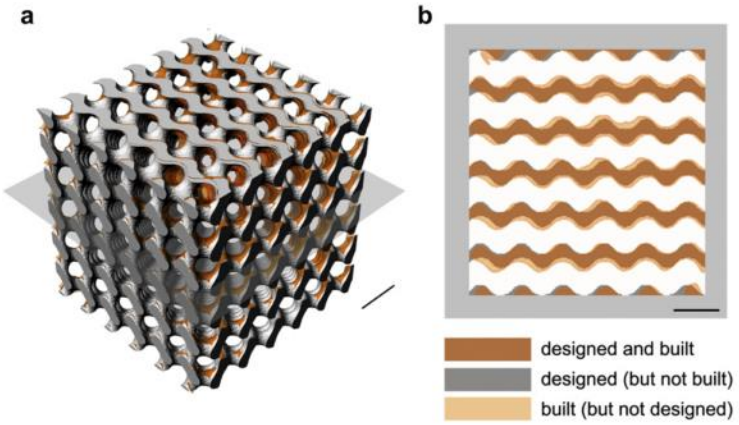

Figure 1:10 3D superposed image of a gyroid cubic scaffold, initial design in grey and constructed structure in orange (Source: Mechels *et al* 2010 [44]).

One of the problems presented in scaffolds fabricated using SL is the formation of a layer stair-stepping effect (Figure 1:11). This effect results from the conversion of the *3D* design model into a set of 2D layers and the layer-by-layer addition process [45]. Recently some techniques have been developed to reduce this effect [45], producing smooth curved surfaces. However, it is considered that this effect is not problematic in the current project and can even be beneficial for initial cell attachment upon seeding due to increased tortuosity.

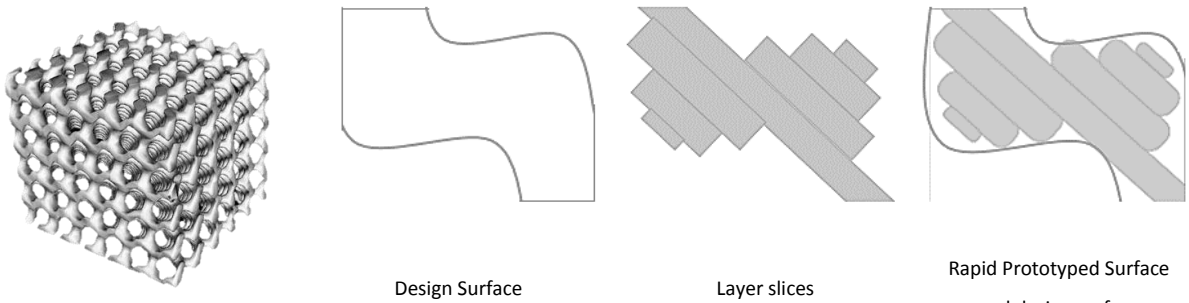

Figure 1:11 Illustration of layer-by-layer additive manufacturing, from the design surface to the prototyped surface. Stair-stepping effect resulting from the additive process.

This type of scaffold fabrication technique is quite advantageous comparing to others mentioned in the section 1.4. SL not only allows the specific control of the scaffold's properties, but it also produces constructs with excellent characteristics, like for example, high porosities and fully interconnected pores, which facilitates nutrient perfusion, essential to ensure cell viability [22], [46]. Traditional fabrication techniques such as salt-leaching, gas-foaming and phase-separation, followed by freeze- drying only allow the regulation of some parameters like porosity or pore size [44]. Stereolithography permits the construction of tailor-made scaffolds, with minimal limitations of design [39], that can be adapted to the needs of each patient [28], [41].

1.5.3.2 Gyroid Architecture

In recent years numerous studies have been conducted regarding the applicability of stereolithography to construct scaffolds for cartilage tissue engineering, since aforementioned this presents several advantages when comparing to the normal techniques. Several architectures have been tested, with differences regarding to cell amount, distribution and functionality of the generated tissue [28].

In 2009 Mechels *et al* developed a gyroid architecture PDLLA scaffold for bone tissue engineering using this technique, their result established that the gyroid architecture allows an excellent cell infiltration due to the construct's open structure and interconnectivity of the pores [47]. Later on the same team showed that, when compared to a salt leached scaffolds, prototyped scaffolds with the mentioned architecture presented a more homogeneous cell distribution and a considerable delay in the formation of an outside coating layer of cells, responsible for clogging the scaffold's pores [41]. Further research was performed to study the applicability of PTMC gyroid structures prepared by stereolithography for cartilage tissue engineering with success [40], [4] [22].

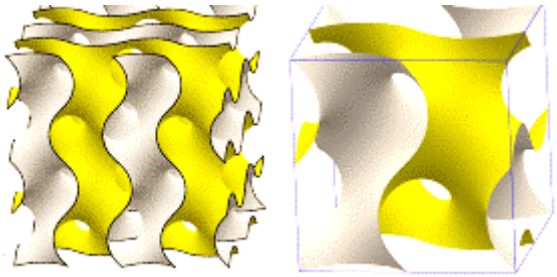

$$\cos x \sin y + \cos y \sin z + \cos z \sin x - C = 0$$

Figure 1:12 Architecture of a gyroid surface [48] and correspondent approximated trigonometric equation (41). Cubic unit of gyroid architecture and gyroid structure formed with cubic repeating units [48].

The gyroid architecture was first discovered in 1970 by Alan Schoen [49], [50] and it is known for being a triply periodic function with infinite connections. The surface of a gyroid architecture can be approximated using a trigonometric equation, that derives from Scwarz and Schoen minimal surfaces structures [41], [49], these are known for having locally a minimal area that results in a mean curvature of zero at every point [44], [51]. Adding a constant number, ***C*** to the trigonometric equation presented in Figure 1:12, it is possible to control in a specific manner the design of the porous architecture. For these reasons the application of this architecture is extremely advantageous, since characteristics like pore size, porosity and surface area may be easily altered so that constructs can closely match the properties of native AF tissue. Furthermore SL of gyroid architectures will allow the construction of custom made implants with the desired shape and size [2].

1.5.3.3 PTMC Poly(trimethylene carbonate)

As mentioned before, the AF is exposed to large loads during physiologic movements, this way a tissue engineered solution for repair of this tissue must be able to sustain loads so that the tissue can recover its bio-mechanical properties. It should also be elastic enough to regain its initial shape after compression. Cross-linked

PTMC macromers of different molecular weights, revealed to be highly flexible and tough, behaving like rubber at room temperature [43]. Compression of solid PTMC constructs presented a compression *modulus* that ranged from 3,1 to 4,2 MPa, with no variation with molecular weight [43] . These results were obtained in a study conducted by Schuller-Ravoo *et al* in 2011, that concluded that PTMC networks are ideal for the creation of biodegradable soft tissue grafts.

Mechanical support is vital for tissue formation and maturation, nevertheless to date few studies take into account the structural and biomechanical properties of the produced scaffold, as some materials possess intrinsic low compression *modulus* and inadequate behaviour when exposed to loads, such as hydrogels. In previous studies conducted by Blanquer *et al* in 2013 [40], porous PTMC gyroid scaffolds were proven to have high compression *modulus* in the dry state, that varied from 0.31±0.09 *MPa* for a 230 *μm* pore size to 0.210±0.030 *MPa* to a 420 *μm* pore size scaffold [40]. These results demonstrated that the smaller pore size scaffolds are indicated for AF reparation, since their compression *moduli* is very similar to that reported in the literature for AF tissue 0.12±0.13 *MPa* to 0.56±0.21 *MPa* [8], [40]. Furthermore it was shown by Schuller-Ravoo *et al* in 2013 that the compression *moduli* increases about 50 *%* in 6 weeks with culture time [22], for a culture of bovine chondrocytes in gyroid scaffolds built with PTMC-based resins.

Although the concrete influence of chemical surface properties of PTMC and other polymers on the AF cells is not clearly known [32], further studies indicated that the natural hydrophobicity and water uptake (≃1,1±0.1 *%*) [39] of PTMC strongly influences interactions between cells and the biomaterials surface, these can also have an advantageous influence in the degradation and mechanical properties of the biomaterial after implantation [43]. In tissue engineering of cartilage it was shown that surface hydrophobicity helps chondrocytes to maintain their differentiated phenotype [39]. Although being composed by a synthetic polymer, PTMC constructs manifested good cell adhesion capabilities [40], [4], [41] that can be further facilitated by lowering the natural hydrophobicity by incubation in culture medium and adsorption of the medium's proteins before seeding [28], [41]. A previous conditioning of PTMC scaffolds in water can increase hydrophilicity, decreasing the water contact angle, most likely due to reorientation or diffusion of the polymer's end groups at the surface [39].

Between the several materials that have been tested for application in tissue engineering of *annulus fibrosus* (see section 1.4), PTMC was proved to be biocompatible, biodegradable by enzymatic surface degradation with non-toxic and non-acidic degradation products that can be excreted by the body's natural pathways [39]. It is also easy to functionalize and presents intrinsic mechanical properties that have been proven to be advantageous for repair of the AF tissue [40]. For these reasons, and because of its applicability in stereolithography, PTMC was the chosen material for the present project.

1.5.3.4 Annulus Fibrosus Cells

In tissue engineering, biocompatibility of the constructs upon implantation is extremely important. Several type of cells have been used in AF repair strategies, mainly mesenchymal stem cell (*MSCs*) and *annulus fibrosus* cells (AFC) from animal or human origin [29].

Although autologous IVD cells are sometimes preferred for this kind of applications, because of its low risk for rejection and unwanted inflammatory responses, collection of autologous cells from a healthy disc is

relatively invasive and may lead to further degeneration of the healthy disc. Furthermore according to a study performed in 2011 by Hegewald *et al* [2], cells collected and isolated from already degenerated IVD (for example herniated disc tissues) present low regenerative potential having limited applications [2].

With regard to the utilization of adult stem cells derived from different parts of the body and embryonic stem cell (ESC), problems related to the required growth factors for precise differentiation of the cells still prevail and intensive research still needs to be performed as well as clinical trials to corroborate the potential of stem cells as a substitute of differentiated cells [32]. This way transplanted stem cells are not adapted to the microenvironment of the degenerated disc, failing at its reparation by shortage of cells and incomplete repair of functionality [52].

In the present study we expect to optimize PTMC scaffold's design characteristics for AF tissue engineering application, for that purpose we have chosen to culture human AF cells, since these will allow to concretely assess the effect of the scaffold's characteristics on cell behaviour, like initial cell adhesion, infiltration and proliferation. [32]. Different types of cells present different responses for the same stimuli and only this way is possible to mimic the conditions to which the construct is subjected after implantation. Note that after implantation of a cellular or an acellular graft, AF cells from the surroundings of the implantation site will infiltrate the scaffold and be responsible for the integration of the construct into the AF environment. In the case of end-stage disc disease the disc is already depleted of endogenous cells and more extensive cellular tissue engineered solutions are required [6].

2. MATERIALS AND METHODS

2.1 PREPARATION OF THE PTMC RESIN AND SCAFFOLDS

All PTMC scaffolds used in this experiment were kindly provided by Sébastien B. G. Blanquer, the presented method is a summary of the synthesis of the mentioned scaffolds [40]. The scaffolds were designed using a *3D* software, Rhinoceros *3D*® (McNeel Europe and K3dSurf).

For preparation of the PTMC resin a two-step reaction was performed. The first step involves the preparation of a hydroxyl-ended PTMC oligomer by ring-opening polymerization (oligomerization) of 1,3-trimethylene carbonate (TMC Foryou Medical®, China), initiated by tri(hydroxymethyl) propane (TMP Sigma Aldrich® Netherlands) and canalized by $Sn(Oct)_2$ (0.05 *wt%*; Sigma Aldrich®, Netherlands) was used. The polymerization was carried-out in an argon protected atmosphere for a total of 3 days at 130 *°C*. Later the resulting oligomer was end-functionalized with methacrylate groups in a 2 days reaction at 120 *°C* with methacrylic anhydride (94 *%*; Sigma Aldrich® Netherlands) at an excess of 50 *mol%* (determined having as reference the amount of functional hydroxyl groups on the molecule) [40], [22]. The resin was then purified using a under vacuum distillation at a maximum temperature of 130 *°C* as described in the literature [22]. The degree of functionalization, rate of conversion and monomer molecular weight were determined by ^1H NMR spectroscopy (Varian Innova® 300 *MHz*, USA).

The PTMC macromer can only be used in stereolithography if it is in a form of a liquid resin with a viscosity of approximately 5 *Pa·s*, because only this way is possible to control the crosslinking process. The mentioned resin was prepared by dilution of PTMC (5000 *g/mol*) in propylene carbonate. Lucirin TPO-L (5 *%wt*) and Orasol Orange dye (0.15 *wt%*; Ciba Specialty Chemicals®, Switzerland) were added to resin, a photo-initiator and a dye for control of the penetration depth, respectively. The photo-polymerization was performed layer-by-layer in an EnvisionTech Perfactory MiniMultilens stereolithography apparatus using a blue light (400-500 *nm*). The layer thickness was 25 μm at a pixel resolution of 16·16 μm^2, the illumination time for layer was 40 seconds with an intensity of 20 mW/cm^2 [40].The resulting constructs are extracted in acetone and dried in acetone until a constant value of weight is reached. Each scaffold was built to be 5 mm^2, considering a 15 *%* of shrinkage after the extraction and drying process. Network characteristics were determined by micro-computed tomography, performed using a eXplore Locus GE µ-CT scanner with a resolution of 8 μm (General Electric®, USA).

Construct were sterilized by immersion on a 70 % (*v/v*) aqueous ethanol solution for 30 minutes, after this period the ethanol was aspirated and remaining liquid was evaporated for 30 minutes. The constructs were washed 6 times with Dulbecco's phosphate buffer solution (DPBS; Gilbco-BRL®, UK). Before seeding the scaffolds were pre-treated with maintenance medium overnight.

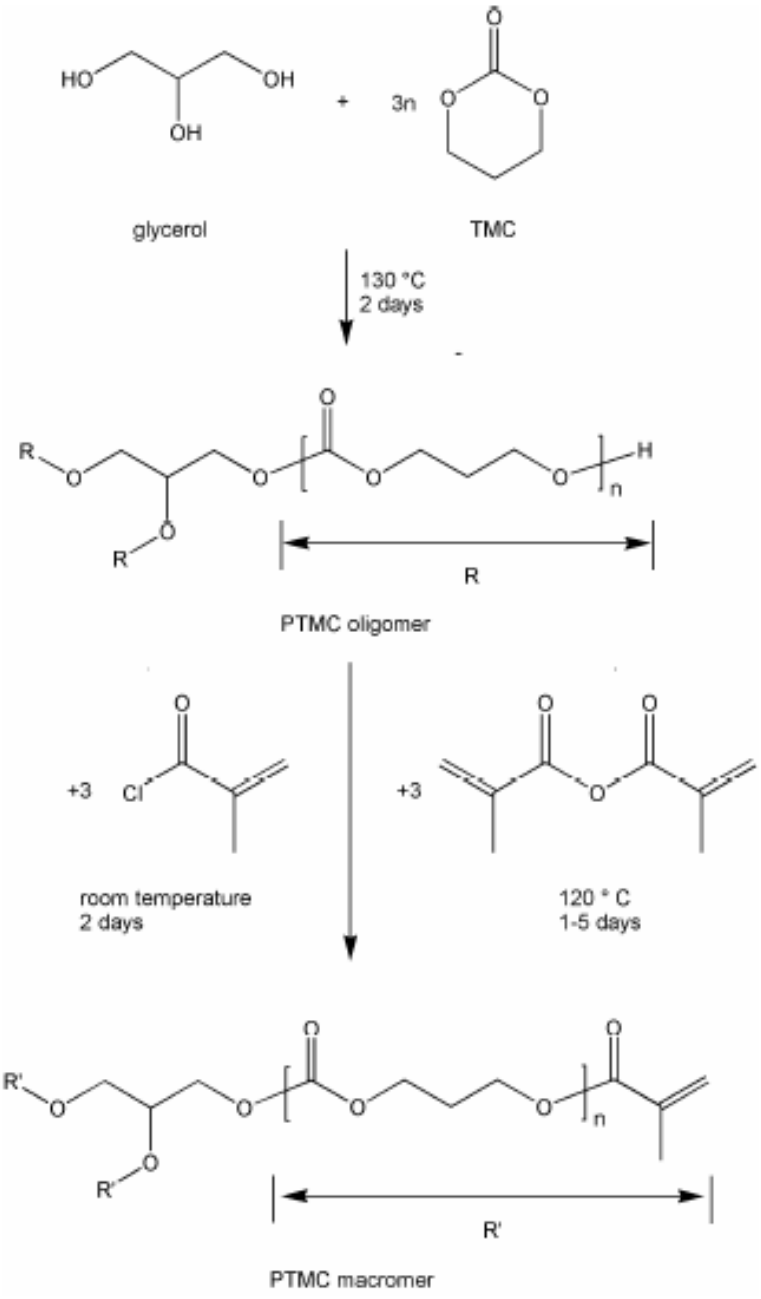

Figure 2:1 Summary of the chemical synthesis of PTMC macromers [39].

2.2 CELL CULTURING AND SEEDING

Human *annulus fibrosus* cells (passage 3; Science Cell, USA) were thawed and expanded in a T75 culture flask, with an expansion medium that consisted in a Nucleus Pulposus Culture Medium (NPCM, Science Cell® USA) supplemented with 2 *%* Fetal Bovine Serum (FBS), 1 *%* Nucleus Pulposus Cell Growth Supplement (NPCGS) and 1 *%* of a Penicillin/Streptomycin antibiotic solution (P/S), all the supplements were obtained from Science Cell®, USA. After 3 days of culture, the flask presented a confluence higher than 80 *%* and the cells were passed into a T175 flasks and cultured for a period of 4 days, after which they were ready for seeding (for further information consult Annex 7.3.1).

Each scaffold was seeded from the top by pipetting a total of 200 000 passage 4 cells, present on a volume of approximately 100 *µL* of cell suspension prepared with NPCM supplemented medium, what corresponds to a seeding density of 2 000 $cells \cdot \mu L^{-1}$. The seeding was carefully carried in a 24 well-plate so that the cell suspension that drained from the PTMC scaffold could be reapplied to the top of the scaffold, ensuring good coverage of its total area and improving the cell distribution upon seeding. The scaffolds were then incubated in the well-plate for 3 hours, after this period 1 *mL* of NPCM supplemented medium was added and the scaffolds were kept under static culture conditions in a humidified air incubator from *SANYO*, with 5 *%* CO_2 at 37 *°C*. Medium refreshments took place every other day by addition of 1 *mL* of the supplemented medium to each well. All cell involving procedures were performed under aseptic conditions in a *CleanAir®* DIN 129880 laminar flow hood (LFH).

2.3 MICROSCOPIC AND HISTOLOGICAL ANALYSES

After 24 hours, 7 days and 14 days of culture, PTMC scaffolds were analysed performing a Methylene Blue staining to evaluate the cell's initial adhesion, proliferation and distribution. This dye stains the acid molecules in the cell's nuclei in a deep blue colour and it also lightly stains the cytoplasm. Samples were washed with DPBS to remove non-adhering cells, fixed with a 3,7*%* solution of paraformaldehyde (PFA; Sigma-Aldrich®, Netherlands) and then stained, each with 4 drops of Loffler's Methylene Blue Solution (LMBS; Sigma-Aldrich®, Netherlands). The samples were rinsed with DPBS after PFA and LMBS applications to take of the excess. Specimens were imaged using a Nikon® SM2-10A stereomicroscope equipped with a Sony® 3CCD camera. Each construct was cross-sectioned with the help of a scalpel, and pictures of the bottom, top and of the cross-section of the scaffolds were taken with several magnifications. A sample was verified for each condition of the constant surface area experiment and the constant pore size experiment.

To determine not only the viability, but also the distribution of the cells a Live/Dead® fluorescent staining (Invitrogen®, USA) was performed. This staining uses small-molecule probes that determine cell viability based on the intercellular activity of esterase and the integrity of the plasma membrane, in one hand Calcein AM is absorbed by living cells staining it green and Ethidium Homodimer-1 (EthD-1) binds to nuclei acids of cells with damaged membranes, producing a red colour. The samples were initially rinsed with DPBS and then incubated for 35 minutes with a DPBS working solution composed by EthD-1 and Calcein AM, with a working concentration

of 0.25 *µM* and 1,00 *µM*, respectively. Samples were visualized using an inverted fluorescence microscope (AMG®, EVOS *ft*) equipped with a Texas Red (TXRed) and a Green Fluorescent Protein (GFP) filter with limits of excitation/emission of 495--635 *nm* to 495-515 *nm*, respectively. Viable cells were identified by its green fluorescence and the dead cells by a red fluorescence, samples were visualized from the top, bottom and cross-section. Due to a lack of samples and dye infiltration problems verified in the first experiment, this kind of analysis was not performed for the second experiment of constant pore size.

2.4 DNA ASSAY

To quantify the amount of cells present in each specimen a CyQuant® proliferation from Life Technologies™ assay was carried out. The scaffolds were first washed with DPBS and then transferred into eppendorfs with 1 *mL* of 0.1 *%* Triton X-100 lysate buffer solution (Sigma-Aldrich®, Netherlands). The samples were hammered and then frozen at a temperature of -80 *°C* and then thawed, this cycle was repeated 2 times after which the scaffold was removed and the samples centrifuged. For determination of the amount of cells, 20 *µL* of each sample's cell suspension was placed in a 96 well-plate with 180 *µL* of CyQuant® working solution, previously prepared with CyQuant GR dye (400*x* diluted) and cell lysis buffer (20*x* diluted), using miliQ water as a solvent. As a blank, 20 *µL* of a 0.1 *%* Triton X-100 lysate buffer solution was used.

The samples fluorescence measurements were performed using a Tecan® Safire 2 microplate reader, at an excitation maximum of 480 *nm* and emission maximum of 520 *nm*. For each of the two first experiments 3 samples of each characteristic (*n*=3), were analysed for each time-point (24 hours, 7 days and 14 days of culture), triple measurements of each sample were performed. A standard curve was created to determine the exact cell number present in each sample using passage 4 hAFC cells, see Annex 7.3.1.

2.5 MECHANICAL TESTING

For the assessment of the mechanical properties of the scaffolds after 1 day, 7 days and 14 of culture, compression tests were carried out at room temperature using a Zwick® Z020 tensile tester armed with a 500 *N* load, data analysis and compression test details were specified using the *Xpert Series* II® software. Each scaffold was compressed until a maximum compression strain of 80 *%* was reached, at a constant velocity of 30 *%* strain per minute. For each sample, the characteristic dimensions (length, thickness and width) were measured using a Mitutoyo® thickness meter (precision 0.01 *mm*), right before the beginning of the compression test. The samples were compressed in a wet state and the compression *moduli* was determined by applying a linear regression to the resultant stress-strain plot, this was made between the values of 7 *%* and 9 *%* strain for all the samples, since for those values the variation of the strain is directly proportional to the applied force resulting in a linear dependence region.

2.6 STATISTICAL ANALYSIS

Statistical analysis was performed using GraphPad Prism 5 software for Windows (GraphPad®, USA). For cell number Cy-Quant® assay, carried out for the experiments of constant surface area and fixed pore size, two-way analysis of variance, ANOVA, was executed. The different scaffolds were analysed and the behaviour of each in the 3 different time-points was compared using a Bonferroni post-test. For the compression tests a one-way ANOVA analysis was performed to analyse the evolution of the mean compression *modulus*. All the results considered significant were present within a set confidence interval of 95 *%*, which means that $P < 0.050$. The error reported in the figures corresponds to the standard deviation (SD) of all the samples to the calculated mean value.

3. RESULTS AND DISCUSSION

As mentioned before the present study is divided into three independent experiments. For the evaluation of the effect of the scaffold's design parameters, qualitative and quantitative analysis were performed whereas for the assessment of the mechanical properties of the scaffold only a quantitative analyse was executed. In order to simplify the results analysis, the following outline is presented. Note that each section is accompanied with the correspondent results discussion.

Table 3:1 Outline of the constant surface area, constant pore size and compression test experiments. Type of output (* further results in Annex 7.4.1).

Chapter	Type of Analyisis	Sub-Chapter	Evaluated parameter	Output
3.1	µ-CT scanning: Scaffold Characterization	-	Pore size, Porosity and Specific Surface Area	Quantitative values
3.2	Methylene Blue Staining: Cell adhesion, distribution and proliferation	3.2.1	Pore size Influence	Qualitative: Stereomicroscope images
		3.2.2	Porosity Influence	
3.3	Live/Dead Assay: Viability and distribution of the cells	3.3.1*	Pore size Influence	Qualitative: Fluorescence Microscope Images
3.4	Cell seeding and culture	-	Pore size and Porosity Influence	Quantitative: Amount of cells
3.5	Mechanical Properties	-	Culture time	Quantitative: Compression *modulus*

3.1 SCAFFOLD CHARACTERIZATION

The network characteristics of the scaffolds (porosity, pore size and surface area) were determined, as mentioned before, using a micro-computed tomography (Figure 3:1). These measurements were performed *a priori* by Sébastien B. G. Blanquer. The present study is divided into three experiments, each with different ranges of scaffolds characteristic, presented in the following tables (Table 3:2; Table 3:3 and Table 3:4).

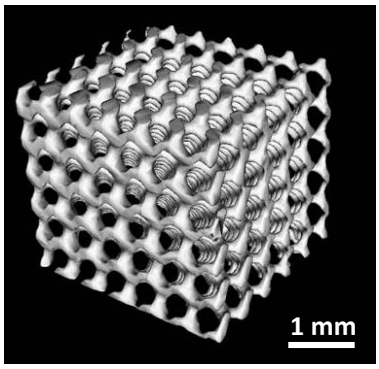

Figure 3:1 Image from micro-computed tomography (µ-CT) of a gyroid architecture PTMC scaffold.

It is important to mention that all of the design parameters of the scaffolds are dependent on each other, thus changing a parameter will have a repercussion in all the other parameters. Aforementioned the material's geometry was defined in order to keep one of the parameters constant and this way analyse the effect of the others characteristics (see Table 3:2 and Table 3:3).

The constructed scaffolds were examined using a scanning electron microscope to check their structure (Figure 3:2), what revealed no inconsistency with the original design. Furthermore, all scaffolds presented a cubic shape with 5 mm^3 (Figure 3:2).

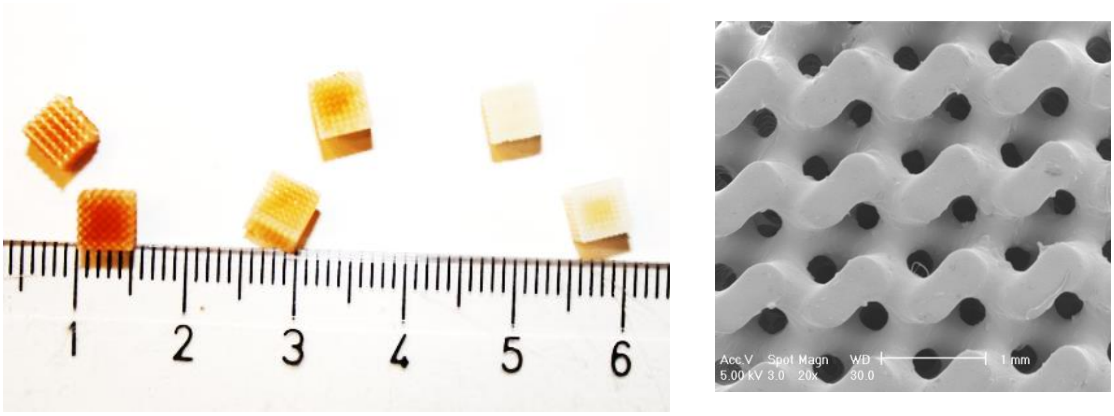

Figure 3:2 On the left side: fabricated PTMC scaffolds with approximately 5 mm^2 each. (Second experiment scaffolds, variation of colour with porosity, increase porosity from the left to the right 57 % to 77%). On the right side: scanning electron microscope examination of a PTMC gyroid architecture scaffold.

Table 3:2 Main characteristics of the scaffolds used for the constant surface area experiments.

Pore size (*μm*)	**Porosity (*%*)**	**Number of pores**	**Specific Surface Area (μm^{-1})**
311	62.0	8	7.00
383	69.0	7	
493	74.7	6	

Table 3:3 Design parameters of the scaffolds used for the constant pore size experiments.

Pore size (*μm*)	**Porosity (*%*)**	**Number of pores**	**Specific superficial area (μm^{-1})**
430	57.0	6	4.66
	67.0	8	7.36
	77.0	10	16.52

Table 3:4 Design parameters of the scaffold used for the test of the mechanical properties.

Pore size (*μm*)	**Porosity (*%*)**	**Number of pores**	**Specific superficial area (μm^{-1})**
400	70.0	6	6.27

3.2 CELL ADHESION, DISTRIBUTION AND PROLIFERATION

As stated before Methylene Blue staining allows to establish a qualitative assessment of cell distribution and proliferation, since all the cells present in a scaffold at a certain time-point are stained blue. The cytoplasm of the cells is also lightly stained blue, enabling to have a rough idea of cell morphology. The staining was carried out for constant surface area and constant pore size experiments, for all time-points.

Observing of the cross-sectioned scaffolds (Figure 3:3 and Figure 3:4), is clear that all the scaffolds present an even distribution of the cells and that these seem to have easily proliferated throughout the scaffold, even in the first time-point (24h after seeding) the adhering cells cover all the scaffold's surface from the top to the bottom. All scaffolds present good pore interconnectivity and are biocompatible with the seeded cells. In both experiments there is an intensification of the staining with increase culture time, indicating that most part of the scaffolds appear to present an increase of the quantity of cells.

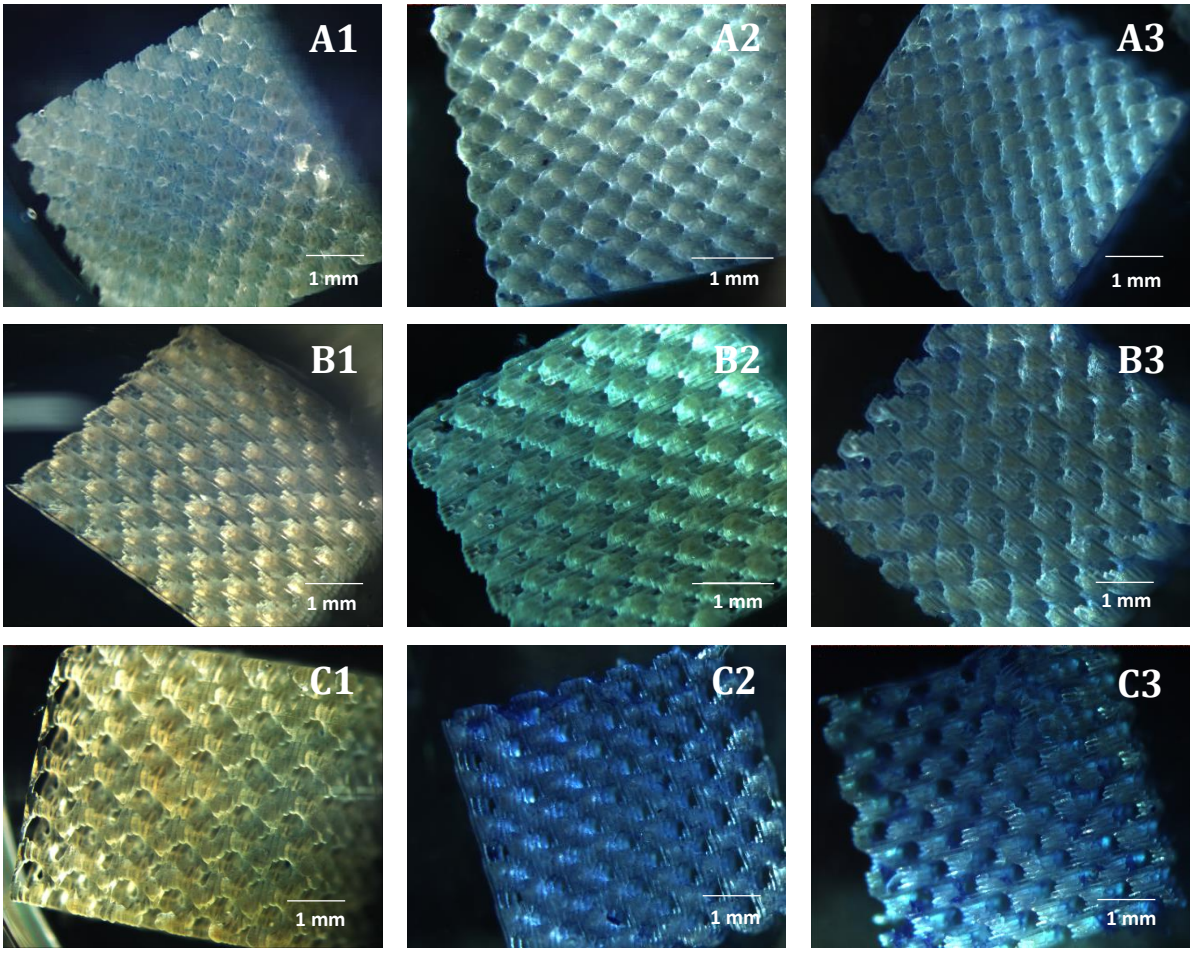

Figure 3:3 Cross-section stereomicroscope images of scaffolds for the constant surface area experiments. Increasing pore size from the top to the bottom (A 311 μm; B 383 μm; C 493 μm). Increasing culture time, from left to right (1- 24 hours of culture, 2- 7days of culture. 3 – 14 days of culture).

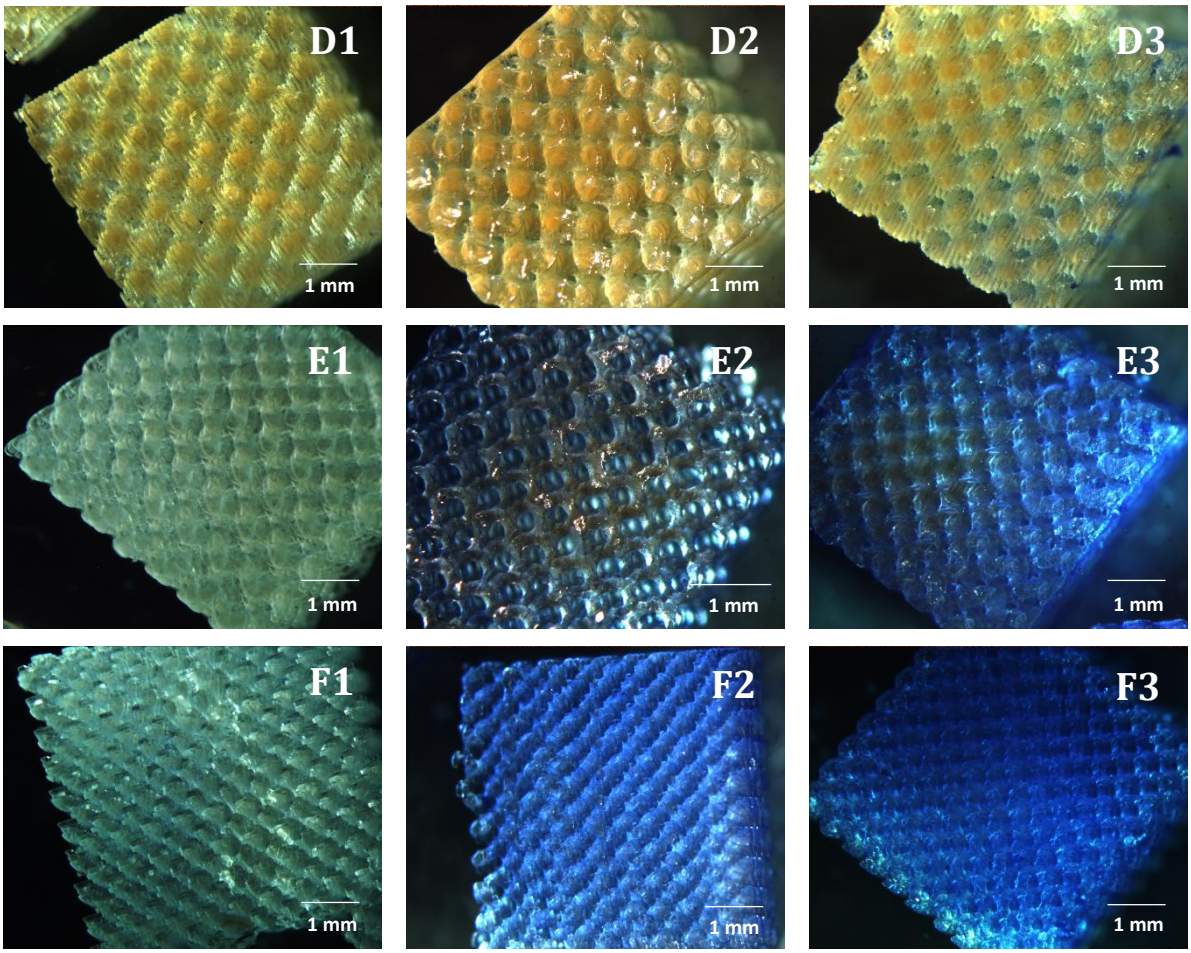

Figure 3:4 Cross-section stereomicroscope images of scaffolds for the constant pore size experiments. Increasing porosity from the top to the bottom (D 57 %, E 67 % and F 77 %). Increasing culture time, from left to right (1- 24 hours of culture, 2- 7days of culture. 3 – 14 days of culture).

3.2.1 Pore size Influence

In the constant surface area experiment the results demonstrate that although the seeding was rather successful for the higher pore sizes of 493 *μm* and 383 *μm* (B1 and C1 of Figure 3:3), the smaller pore size scaffold seems to present a slightly uneven distribution of the cells in the first time-point, presenting more cells on the top and fewer on the bottom. The attained results indicate that for smaller pore sizes (≤ 311 *μm*) the employed seeding technique is not truly efficient (A of Figure 3:5). This fact can be directly related to the static seeding conditions in a narrower pore and the scaffold intrinsic hydrophobicity, from the building material PTMC [(40), (41), (53),] which hinders the penetration of the cell suspension throughout the scaffold. Nevertheless, although not being initially regularly distributed, 7 days after seeding the 311 *μm* pore size construct manifest a good scattering of the cells, indicating that these can easily proliferate, changing the initial tendency.

After 24 hours of seeding, the bigger pore size scaffold (493 μm) appears to present a less intense stain when compared to smaller pore constructs (Figure 3:3). Usually in large enough pores there is a risk of migration of the cells straight though the scaffold, due to reduced surface area for attachment [54]. However, in the present study this effect was minimized by the protuberances in the several layers formed by the stair-stepping effect, since these tortuous channels increased the residence time of cells inside the scaffold, being more likely to contact with the scaffold's surface [46].

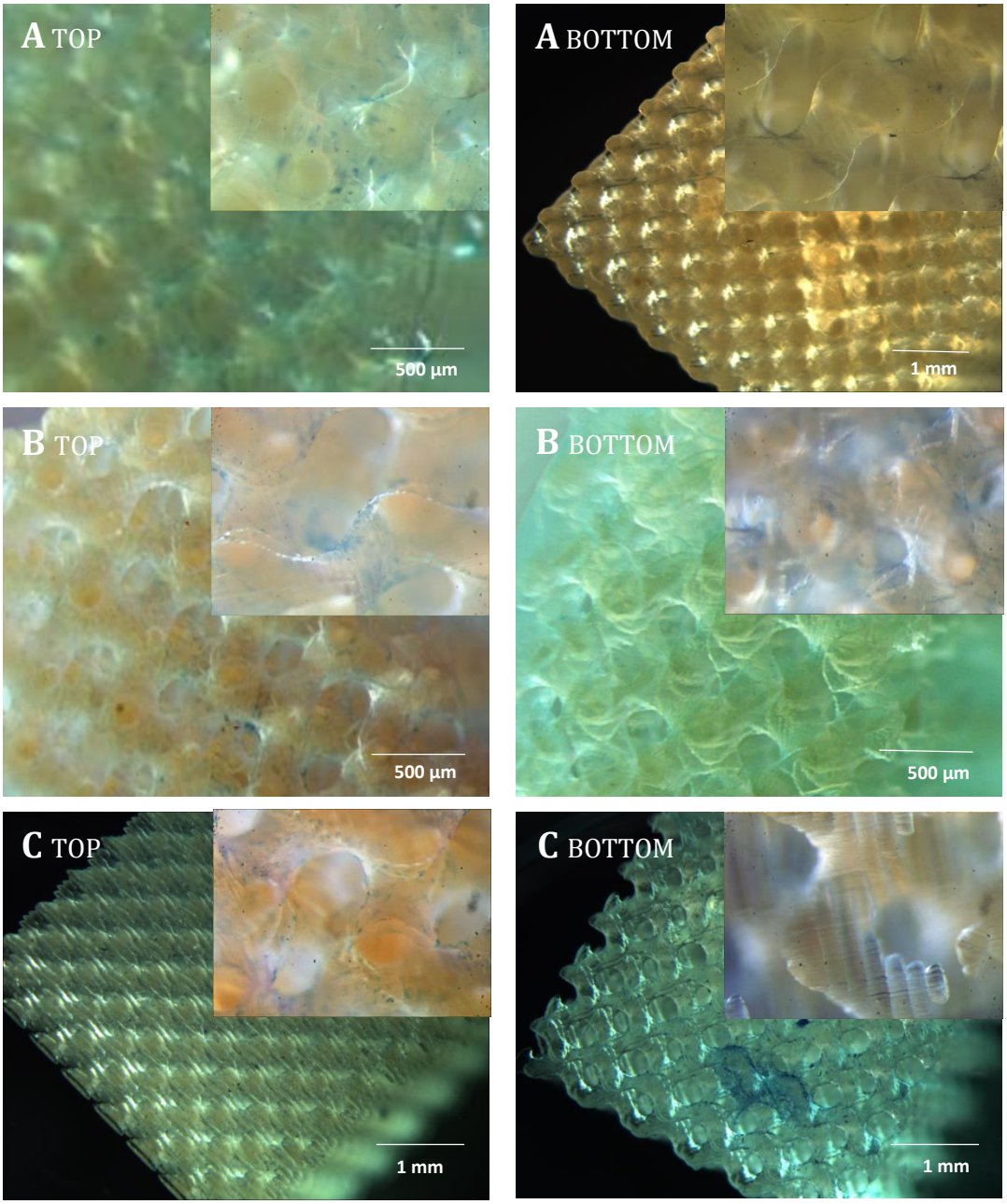

Figure 3:5 Stereomicroscope images of methylene blue staining of the top and bottom of the scaffolds after 24 hours of culture, detailed view of the cells. Increasing pore size from the top to the bottom (A -311 μm; B - 383 μm; C- 493 μm).

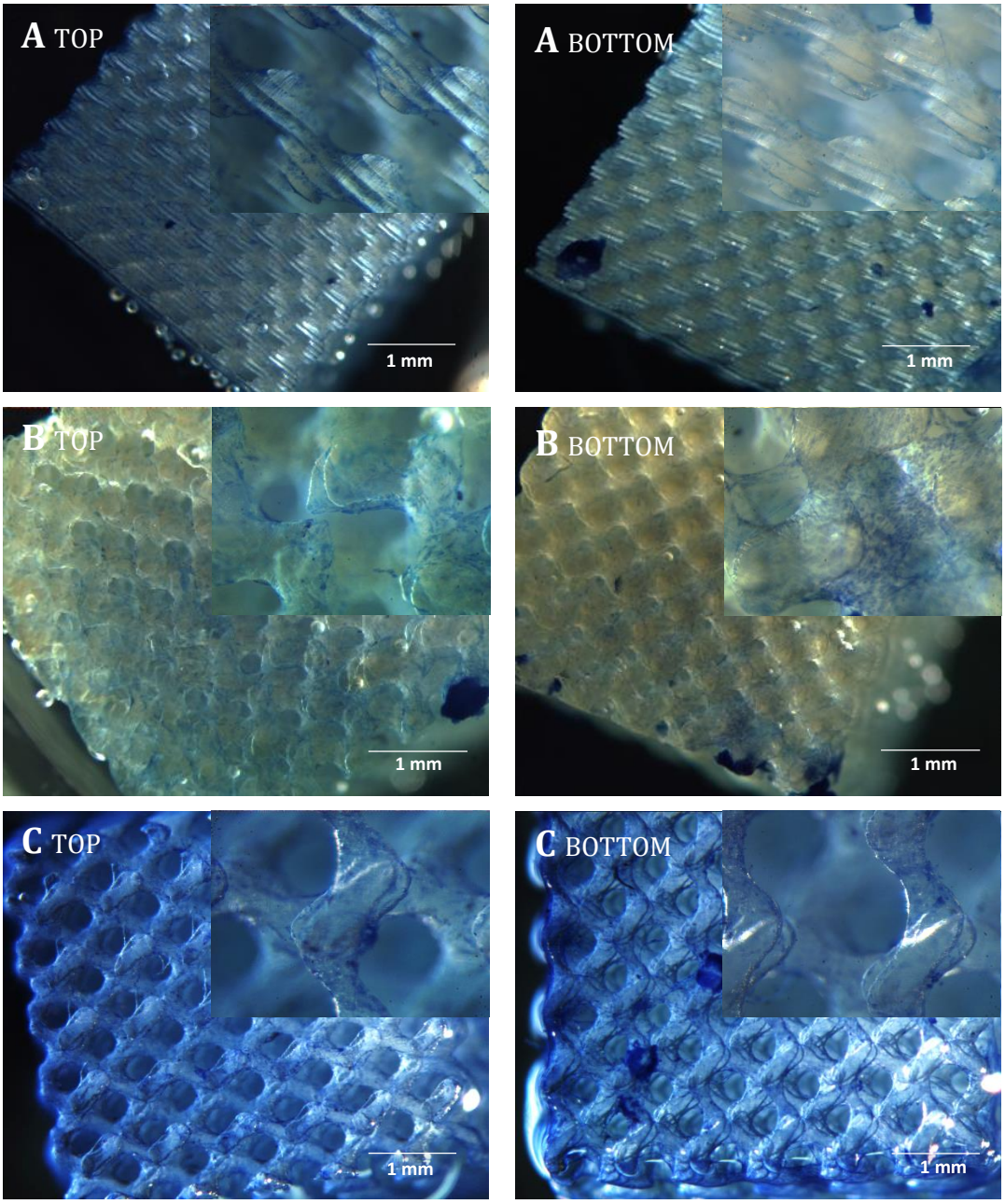

Figure 3:6 Stereomicroscope images of methylene blue staining of the top and bottom of the scaffolds after 7 days of culture, detailed view of the cells. Increasing pore size from the top to the bottom (A - 311 μm; B - 383 μm; C - 493 μm).

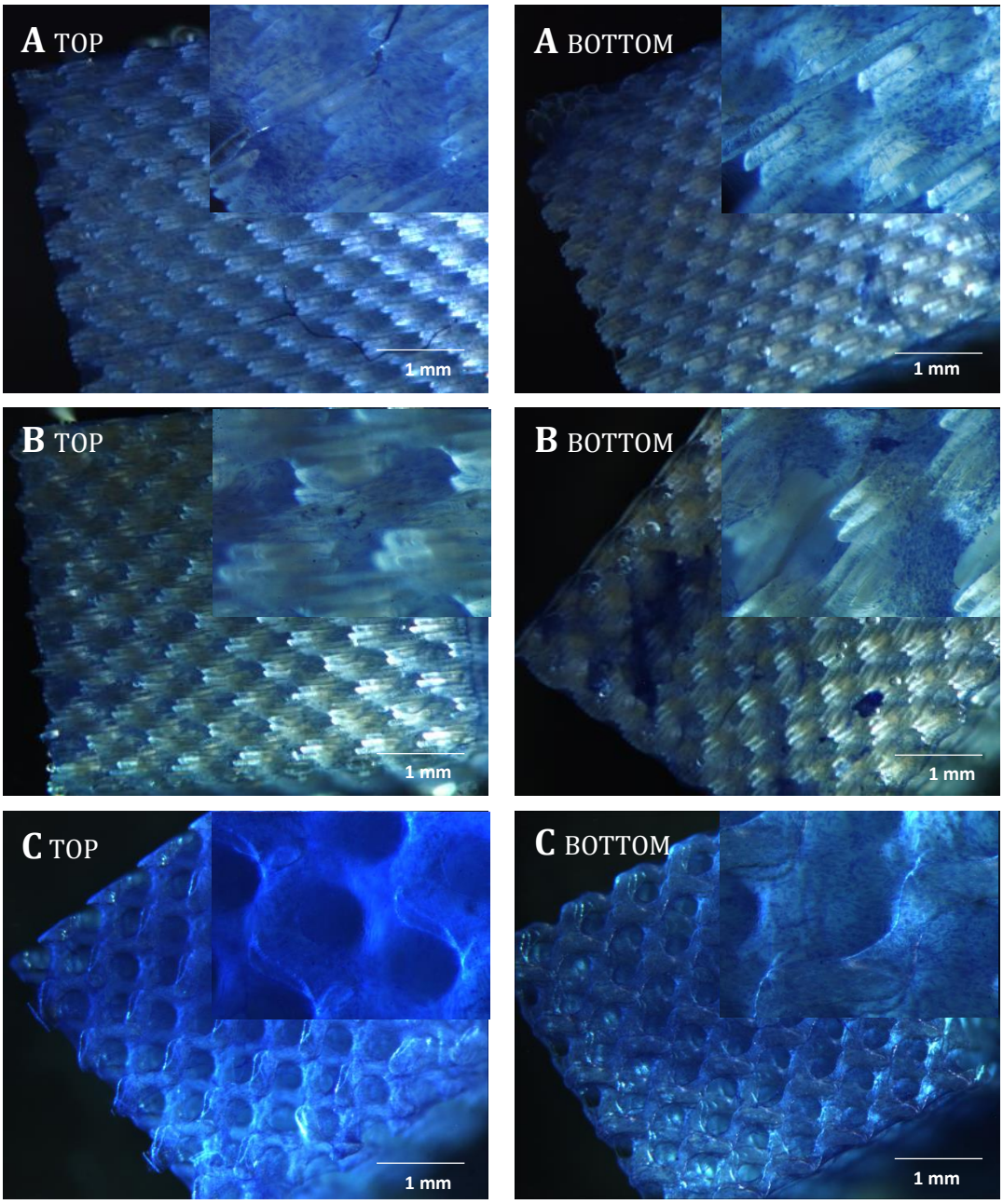

Figure 3:7 Stereomicroscope images of methylene blue staining of the top and bottom of the scaffolds after 14 days of culture, detailed view of the cells. Increasing pore size from the top to the bottom (A- 311 μm; B - 383 μm; C- 493 μm).

Overall analysis of constant surface area scaffolds in the different culture times indicates an apparent increase of the cell amount with culture time for all constructs (Figure 3:5, Figure 3:6 and Figure 3:7). Nonetheless for longer periods of culture, the different scaffolds exhibit an increasing difference in terms of cell proliferation and bigger pore size scaffolds (≥ 383 μm), seem to possess greater numbers of cells.

In terms of cell behaviour, one can observe that initially, after 7 days of culture, in bigger pore size scaffolds (493 μm) cells start to proliferate covering the surface of the scaffold's backbone structure. After covering all the structure, the cells started to elongate and filling the pores. Contrariwise, in smaller pore sizes (311 μm) the proximity between pore's walls facilitated the lengthening of the cells to establish a connection between the different points in the structure shortly after seeding, readily covering the pores. After 7 and 14 days more cells seem to proliferate on the outside of the scaffold. This early variance on cell behaviour can influence the supply of nutrients and oxygen to the inside of the scaffold and thus influence cell amount and cell viability, these aspects will be discussed further in the chapter 3.4 of quantitative analysis of cell numbers.

After 14 days of culture the cells form tissue-like structures throughout the scaffolds, this can be observed in all pore sizes on the outside part of the scaffolds. However only the larger pore scaffolds (≥ 383 μm) were completly and homogeneously filled with cells on the inside as it can be observed on the cross-section pictures (Figure 3:3).

3.2.2 Porosity Influence

All constructs evaluated in the second experiment displayed an even distribution of the cells and a good initial adherence. Since all the scaffolds used for this experiment had a fixed pore size of 430 μm, no problem related to the cell seeding has been observed. Nevertheless results are less conclusive than the ones observed for the constant surface area experiment, since the two higher porosity constructs (67 *%* and 77 *%*) demonstrate similar results and both scaffolds appear to be equally complete with cells, particularly after 7 and 14 days of culture.

The lower porosity scaffold (57 *%*) presents an erratic behaviour when compared to the other scaffolds, with a less clear evidence of an increase in cell number with culture time. Also, analysing Figure 3:9 and Figure 3:10, that corresponds to a culture time of 7 and 14 days, respectively, is possible to observe that for this porosity value there was a formation of cell aggregates on the bottom side of the constructs. Because no evidence of aggregate formation was observed after 24 hours of seeding (Figure 3:8), it is presumed that the cell aggregates present in the bottom of the scaffold of culture were a result of static culture conditions in the well-plates, being less evident in the other constructs due to better cell proliferation and distribution.

The cells present a similar behaviour in all the scaffolds, covering their structure first and only forming tissue-like structures that covers the pores after 7 days of culture. The attained results suggest that porosities within the range of this study (57-77 %), had a minor influence on cell behaviour when compared to pore size, once bigger pore sizes like the one used for the constant pore size experiment (430 μm), difficult the direct covering of the pores.

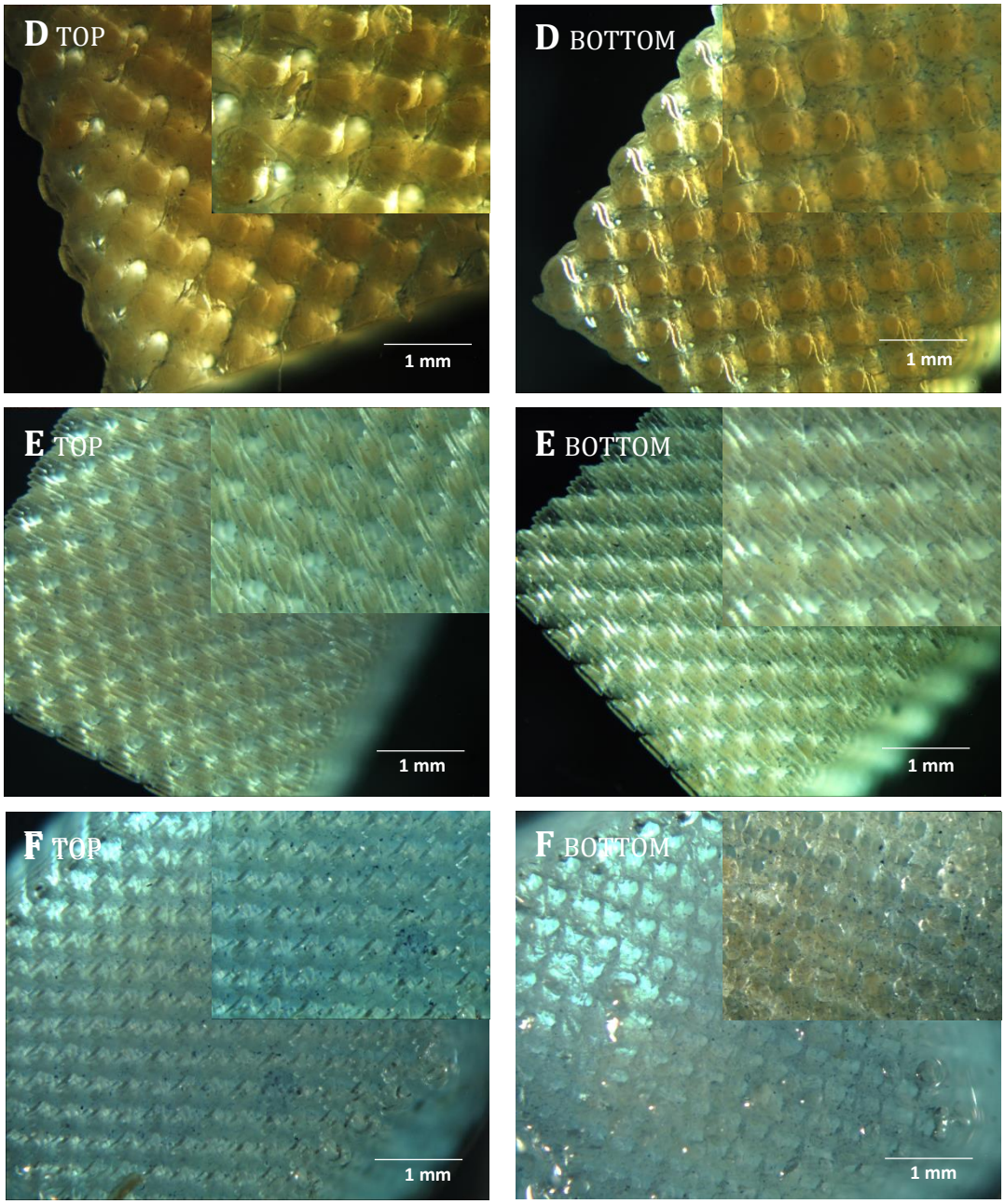

Figure 3:8 Stereomicroscope images of methylene blue staining of the top and bottom of the scaffolds after 24 hours of culture, detailed view of the cells. Increase porosity from the top to the bottom (D - 57 %, E- 67 % and F- 77 %).

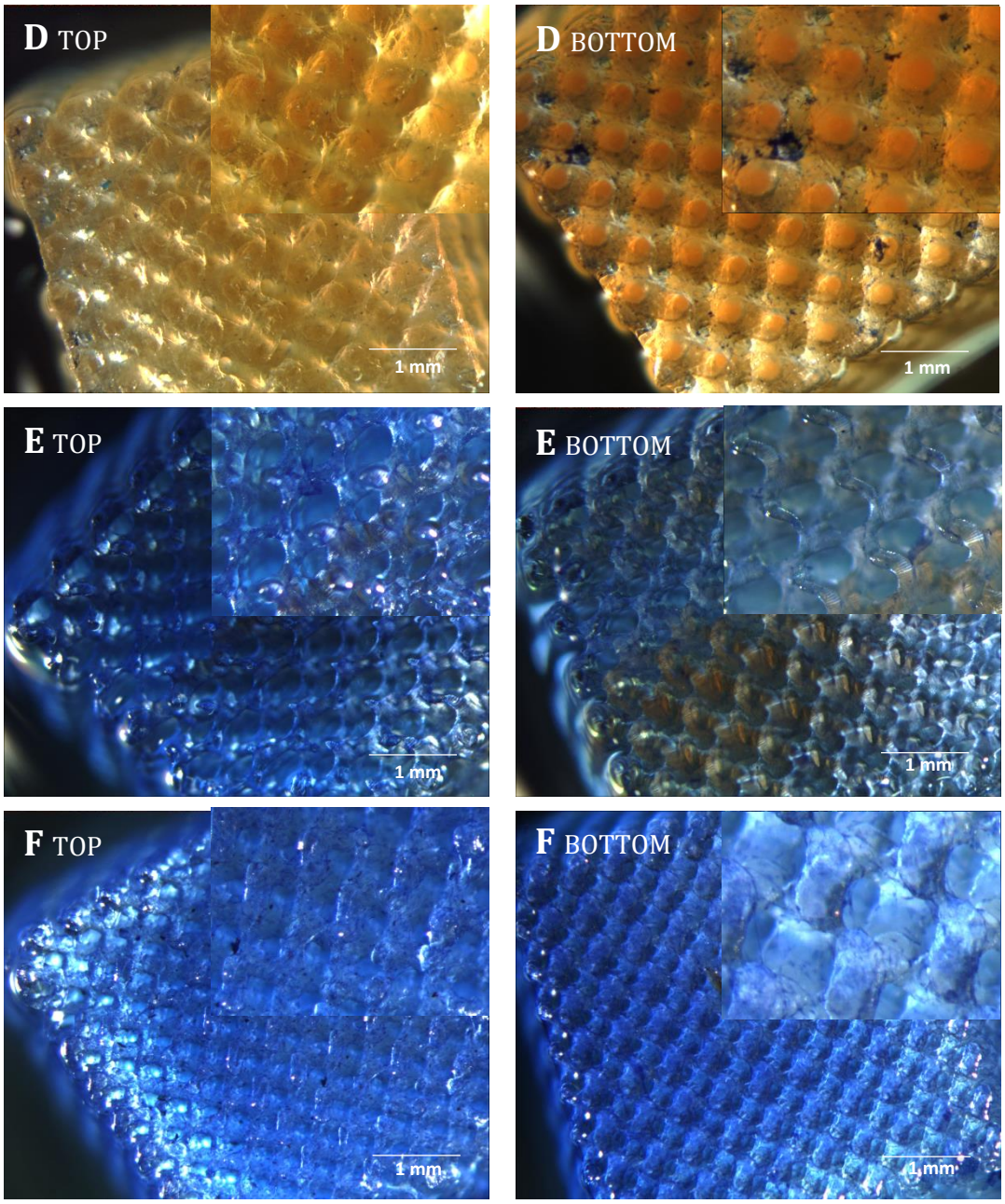

Figure 3:9 Stereomicroscope images of methylene blue staining of the top and bottom of the scaffolds after 7 days of culture, detailed view of the cells. Increase porosity from the top to the bottom (D - 57 %, E - 67 % and F - 77 %).

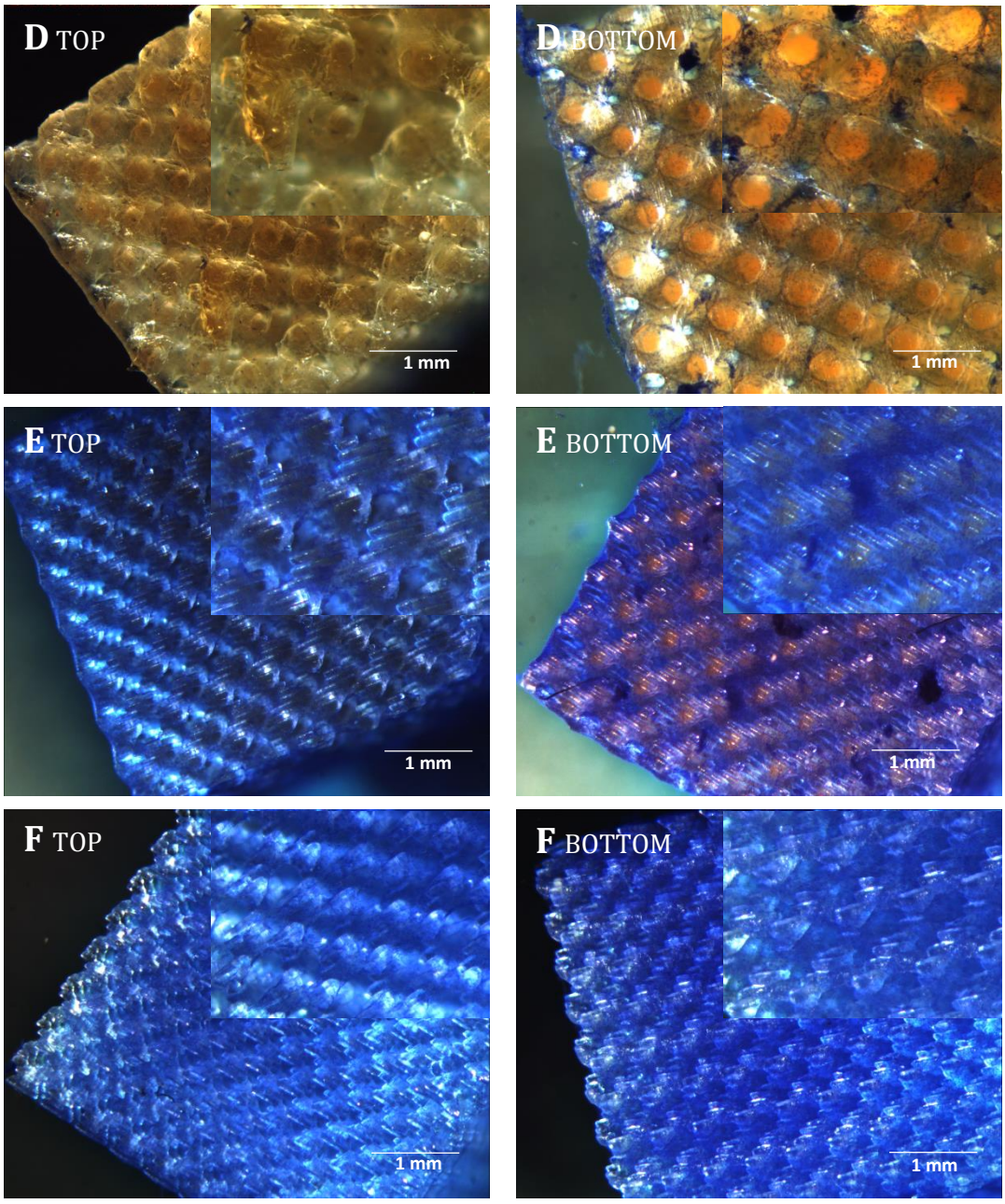

Figure 3:10 Stereomicroscope images of methylene blue staining of the top and bottom of the scaffolds after 14 days of culture, detailed view of the cells. Increase porosity from the top to the bottom (D - 57 %, E - 67 % and F - 77 %).

3.3 VIABILITY AND DISTRIBUTION OF AF CELLS

In order to assess the viability of the cells with cell culture time and as a complement of the methylene blue staining, Live/Dead® two colour fluorescence staining was performed for the constant surface area experiment in all the different 3 time-points (24 hours, 7 days and 14 days). As mentioned before this staining distinguishes the living cells from the dead cells, staining the first ones green and the last red. Furthermore, due to the higher contrast obtained and better image resolution, it allows the evaluation of the morphology and orientation of the cells. All the pictures were taken using an overlay mode, so that there is a superposition of the images given by the Texas Red and Green Fluorescence Protein lens.

This kind of staining was only performed on the first experiment since there was a limitation on the number of scaffolds available. Is relevant to point out that this type of staining does not involve any sort of cell fixation, so the imaging must be readily executed in a way that causes minimal damage to the cells present in the scaffold. Also, there is not a chance of re-staining the scaffolds after the first imaging since the incubation procedure leads to the detachment of most of the cells. For these reasons and because a problem with dye infiltration was observed in lower pore size scaffolds (311 μm) and longer culture times, only methylene blue staining was performed on the second experiment.

3.3.1 Pore Size Influence

No dead cells were observed at any time-point, meaning that the cells, even inside the scaffold, remained viable and had access to all the needed nutrients (please consult annex 7.4.1 for further results). As mentioned before, with increased culture time there is an increase of cell number that can be observed in the cross-section images taken of the scaffolds, Figure 3:11. It has also possible to confirm and visualize with more precision, the previously reported behaviour and proliferation tendency of the cells, present on the chapter 3.2.1. Nevertheless after 14 days of culture, dye diffusion problems were evident, since the cells inside the constructs appear only as shades, being hardly noticeable (Figure 3:11). This is caused by the filling of the porous structure in the smallest pore size scaffolds (≤ 383 μm). Similar results were observed right after 24 hours of seeding for the 311 μm pore size scaffold, revealing that smaller pores are in an early stages connected to poor diffusion. This effect can became problematic overtime, with the increment of cell density that comes with longer culture times, in extreme cases it can lead to a shortage of needed nutrients and oxygenation.

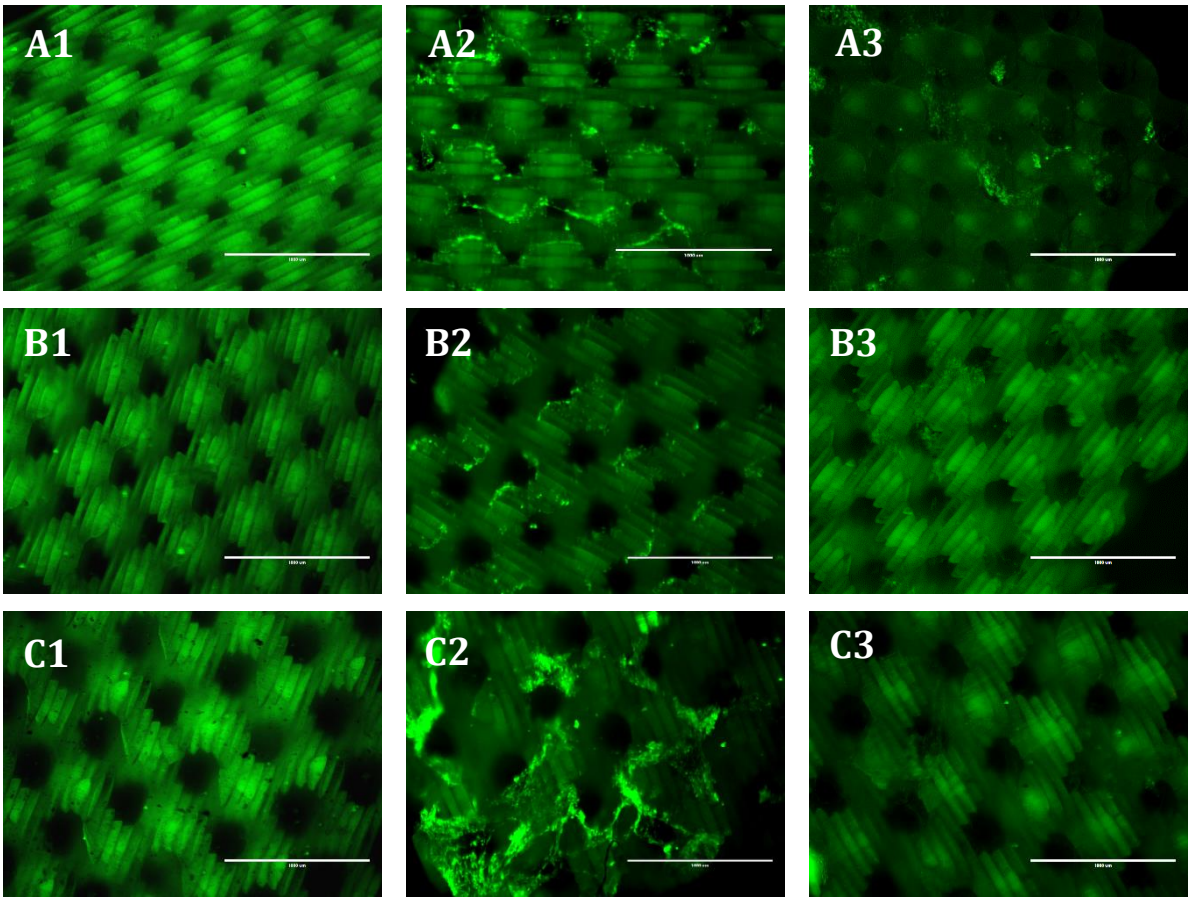

Figure 3:11 Cross-section pictures of the Live and Dead® fluorescence stained scaffolds for the constant specific surface area experiments, with live cells are stained green and dead cells stained red. Increasing pore size from the top to the bottom (A -311 μm; B - 383 μm; C -493 μm). Increasing culture time, from left to right (1- 24 hours of culture, 2- 7days of culture. 3 – 14 days of culture).

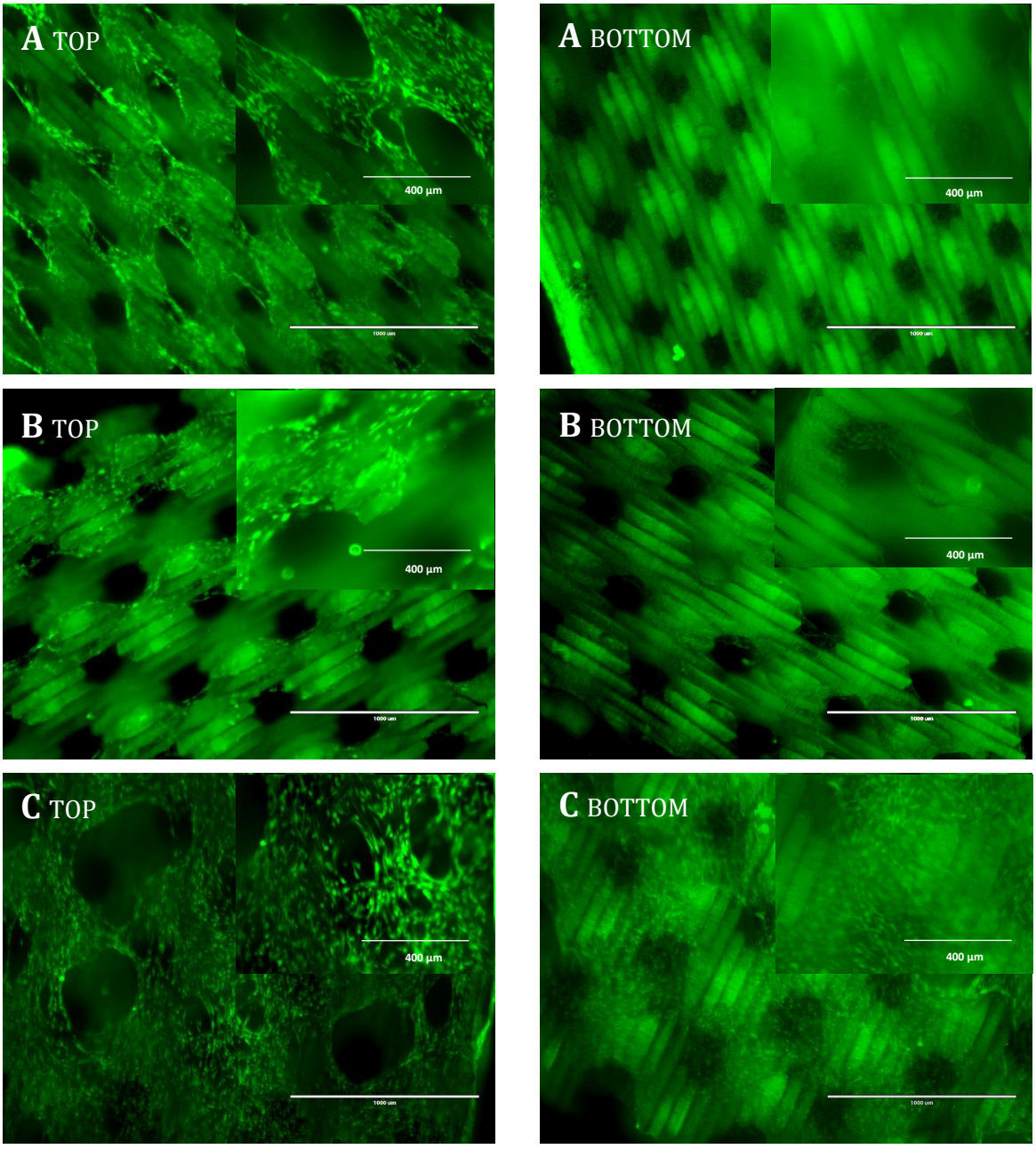

Figure 3:12 Live and Dead® fluorescence staining microscopic images of the top and bottom of the scaffolds after 14 days of culture, detailed view with live cells stained green and dead cells stained red. Increasing pore size from the top to the bottom (A - 493 *µm*; B - 383 *µm*; C -311 *µm*).

Microscopic images taken of the scaffold's top and bottom illustrates with more precision the tendency of growth of the cells overtime and the morphology of the formed structures (Figure 3:12). A difference between the several scaffolds is noticeable, especially after 14 days of culture, the 493 *µm* pore size scaffold presents a much higher number of cells and better cell distribution, when compared to the smaller pore size scaffolds (≤383 *µm*). Analysis of the side of the 311 *µm* pore size scaffold, indicates that after 14 days of culture, the cells that adhered to the well-plate, start to proliferate upwards, forming a thin layer of cells that covers the construct, clogging the pores (Figure 3:13), aggravating the previously discussed diffusion problems into the interior of the

scaffold. These structures form high cell density zones that are intensity dyed and can be visualized from the top and bottom of the scaffolds. An analogous effect was also observed for the 383 *μm* pore size scaffold but at a much smaller scale.

Higher magnifications reveal that the cells cultured in the *3D* environment of the PTMC scaffold, present a morphology equal to that of the initially expanded cells (Annex 7.3.1), correspondent to that described for the cells in the outer AF, being ellipsoidal with long axes. These results are important once they demonstrate that there was not loss of cell morphology, even after 14 days of static culture, validating as well the culture conditions and expansion medium implemented.

Proliferating cells appear to be aligned to form tissue-like structures, growing mainly in a perpendicular manner to the prototyped surface characterized for the stair-stepping effect (Figure 3:14). This effect seems to be beneficial, since the tortuous channels provided support for cell attachment and proliferation.

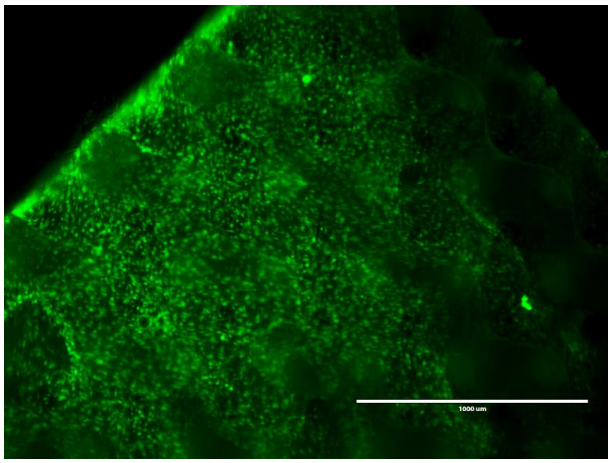

Figure 3:13 Live and Dead® fluorescence staining microscopic images: formation of cell aggregates covering the outside of the 311 *μm* pore size scaffold after 14 days of culture

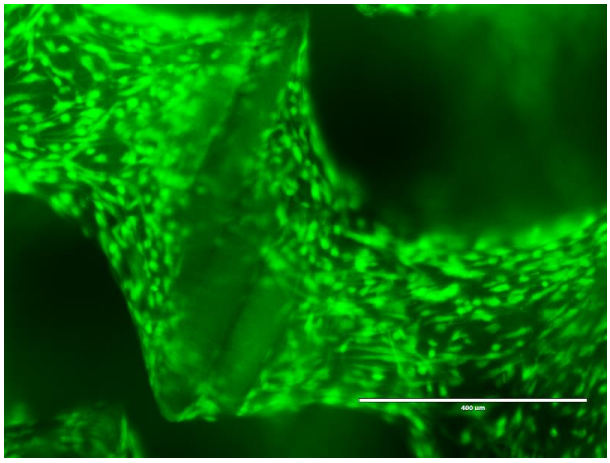

Figure 3:14 Live and Dead® fluorescence staining microscopic images: Oriented cells filling the scaffold's walls. Bottom of the 493 *μm* pore size scaffold after 7 days of culture.

3.4 CELL SEEDING AND CULTURE

The amount of cells present at each time in a determined scaffold was quantified using a Cy-Quant® proliferation assay, which allows to compare cell adhesion and proliferation in the different scaffolds. This assay was only performed for the two first experiments, detailed statistical results may be consulted in Annex 7.4.2.

As mentioned before, the scaffolds used on the first experiment presented a constant value of surface area, with different pore sizes and porosities. All scaffolds presented a tendency of cell growth overtime. When it comes to cell adhesion, the constructs displayed similar cell behaviours, since only a small raise in terms of the number of cells between the scaffold with 383 μm and the one with 493 μm pore size was observed after 24 hours from seeding ($P<0.05$). This was apparently not correlated with the scaffold's design specifications, since no significant difference was observed between the bigger and the smaller pore size scaffold, with 493 μm and 311 μm, respectively.

With culture time, after 7 and 14 days, the bigger pore size scaffold (493 μm and 74,70 %,) presents, as expected, better results in terms of cell growth rate and proliferation, when compared to the smaller pore size scaffolds (≤ 383 μm). This reveals a tendency of increased cell amount for bigger pore sizes, with statistically relevance ($P<0.001$), consistent with the results previously obtained by Sébastien Blanquer *et al* in 2013, when analysing the adhesion and proliferation of hAFC in gyroid PTMC scaffolds, with a range of pore sizes from 230 μm to 420 μm. Both studies follow the already studied preference for bigger pore sizes (380 μm to 405 μm) of chondrocytes and osteoblasts. The raise of cell amount can be related to the increase of two parameters on the scaffold's design, pore size and porosity, however it is expected that the increment of the pore size plays a bigger rule, since between the 63 and 64 scaffold there is only an increase of 7,6 % of the value of porosity (from 69,9% to 74,7 %) and a 22,3 % increase in the pore size (from 383 μm to 493 μm).

These results are also concordant with the results obtained in the methylene blue staining, corroborating the hypothesis that in constructs with bigger pore sizes there is a more efficient diffusion of oxygen and nutrients to the cells inside the scaffold and improved removal of harmful metabolites resultant from cellular activity. It was also verified in the present study, that bigger pore size scaffolds did not present cell aggregates in the outside edges of the constructs, on the contrary to smaller pores, what according to O'Brian *et al* [54], [55] , improves cell migration and proliferation into the centre of the scaffold.

Aforementioned, smaller pore size scaffolds (311 μm) presented cell aggregates and thin layers of cells covering the constructs as shown in Figure 3:13, what in addition to poor nutrient diffusion may also have been responsible for the inhibition of cell growth, through intracellular signalling, which is usually more frequent in smaller pore sizes [56]. More importantly, structures with low porosity and pore size are not able to contain as many cells as larger pores, what can lead to insufficient ECM production and consequently prompt alterations on the cell growth and behaviour [56].

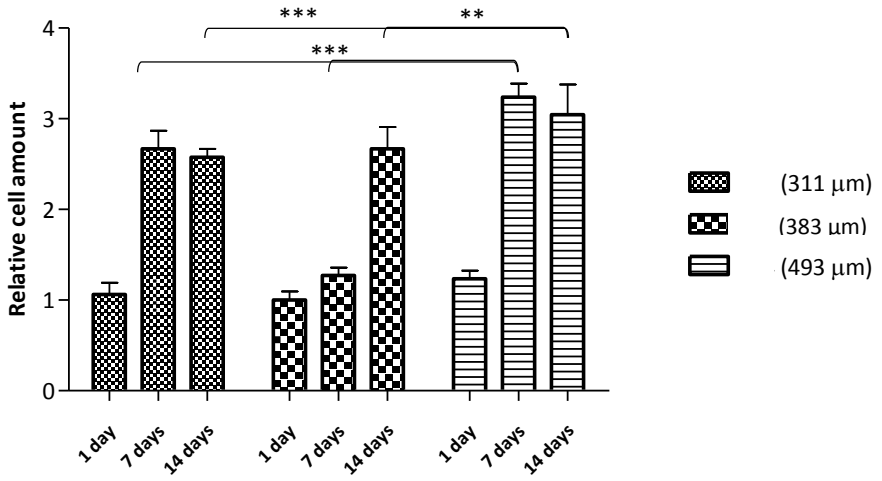

Figure 3:15 Relative cell amount for the scaffolds with constant surface area (7 μm^{-1}), variation with time of culture under static conditions. The error bars correspond to the value of standard derivation of each sample with n=3 (in terms of statistical relevance *** corresponds to P<0.001;** to P< 0.01 and * to P< 0.05).

Table 3:5 Total amount of cells present in the scaffolds with constant surface area (7 μm^{-1}), variation with time of culture under static conditions. Values presented with the correspondent standard deviation.

Scaffold	Time of Culture	Cell Amount
62	24 hours	$(1.83\pm0.22)\cdot10^5$
	7 days	$(4.60\pm0.34)\cdot10^5$
	14 days	$(4.43\pm0.16)\cdot10^5$
63	24 hours	$(1.72\pm0.17)\cdot10^5$
	7 days	$(2.19\pm0.15)\cdot10^5$
	14 days	$(4.59\pm0.42)\cdot10^5$
64	24 hours	$(2.13\pm0.16)\cdot10^5$
	7 days	$(5.57\pm0.25)\cdot10^5$
	14 days	$(5.24\pm0.57)\cdot10^5$

In the second experiment, the results obtained in the quantification of the number of cells were also similar to those accomplished in the methylene blue staining, which revealed higher cell numbers for the highest porosities (≥ 67 %).

As mentioned before and as presented in the section 3.1 of scaffold characterization, for fixed pore size and increasing porosity constructs there is also a raise in the value of specific surface area. The results obtained for the constant pore size experiment demonstrate an increase of cell attachment between the scaffolds with a porosity of 57 % and 67 %, what corresponds to an increase in the specific surface area value from 4.7 μm^{-1} to 7.4 μm^{-1}. Cells in scaffolds with larger surface areas have more space and a greater amount of ligands available

for attachment on the scaffolds [54], these usually also present better cell proliferation and more uniform cell distribution [54], [57]. However for the bigger porosities 77 *%*, this tendency was not observed although there is an raise of over two times the value of specific surface area, reaching 16,5 μm^{-1}. This fact is intimately related with the scaffolds hydrophobicity and high porosity, which in seeding process causes the liquid cell suspension to pass through the scaffold with only retention of small amounts of cell suspension. Furthermore in constructs with higher porosities is easier to detach the cells from the scaffold's structures and a diminishment of the number of cells is expected after washing the scaffolds for DNA quantification.

Analysing cell proliferation, both the scaffold with 67,0 *%* and the scaffold with 77,0 *%* porosity exhibit higher amounts of cells after 7 and 14 days, when comparing to the 57,0 *%* porosity scaffold with $P<0.05$, see Figure 3:16 and Annex 7.4.2.2 for statistical results. This demonstrates that higher values of porosity (≥ 67*%*) have improved cell proliferation rates and better cell distribution. With culture time the effect of the specific surface area and porosity between the 55 and 56 scaffolds becomes less relevant [54], and both scaffolds present comparable results, with no relevant difference between them, in parallel to the results obtained in the studies conducted by Rotman in 2013, when testing the same scaffolds under the same conditions [4]. High porosity and interconnection of pores is this way extremely important for diffusion of the nutrients from the medium and adequate ECM production, benefiting cell growth similarly to the first experiment, were the scaffold with higher porosity (74,7 *%*) also exhibited better distribution and spreading of the cells.

Although there is an increase of the cell amount with culture time, after 14 days all the scaffolds present a non-significant decrease in the cell amount, this may be associated with errors upon cell quantification The 57 % porosity scaffold presents significantly less cells on the third time-point, after 14 days of culture, being possible that the growth of cells around the scaffold has led to a limited diffusion of nutrients into the scaffold, leading to growth arrest or even death. However no viability assay was performed on the second experiment and no further assumptions can be made.

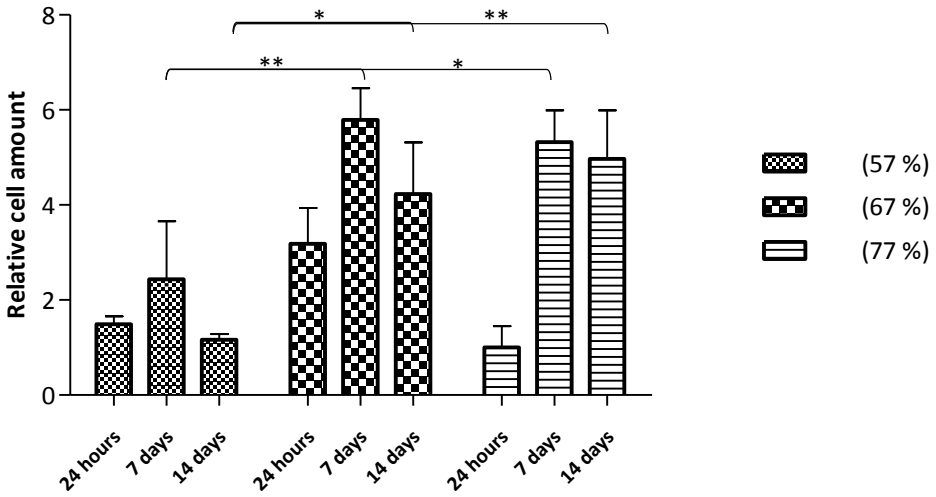

Figure 3:16 Relative cell amount for the scaffolds with constant pore size (430 μm), variation with time of culture under static conditions. The error bars correspond to the value of standard derivation of each sample (In terms of statistical relevance *** corresponds to $P < 0.001$;** to $P < 0.01$ and * to $P < 0.05$).

Table 3:6 Total amount of cells present in the scaffolds with constant pore size (430 μm), variation with time of culture under static conditions. Values presented with the correspondent standard deviation.

Scaffold	Time in Culture	Cell Amount
54	24 hours	$(0.89\pm0.10)\cdot10^5$
	7 days	$(1.44\pm0.72)\cdot10^5$
	14 days	$(0.69\pm0.07)\cdot10^5$
55	24 hours	$(1.88\pm0.44)\cdot10^5$
	7 days	$(3.42\pm0.39)\cdot10^5$
	14 days	$(2.50\pm0.64)\cdot10^5$
56	24 hours	$(0.59\pm0.26)\cdot10^5$
	7 days	$(3,14\pm0.39)\cdot10^5$
	14 days	$(2.93\pm0.61)\cdot10^5$

3.5 MECHANICAL PROPERTIES

The determination of the scaffold's mechanical properties is one of the most important phases of scaffold characterization and is extremely determinant regarding its applicability in tissue engineering. Compression tests were performed for a scaffold with 4000 μm pore size and 70 *%* porosity, the compression *modulus* for wet scaffolds with different cell culture times were obtained for a temperature of approximately 37 *°C* (Figure 3:17).

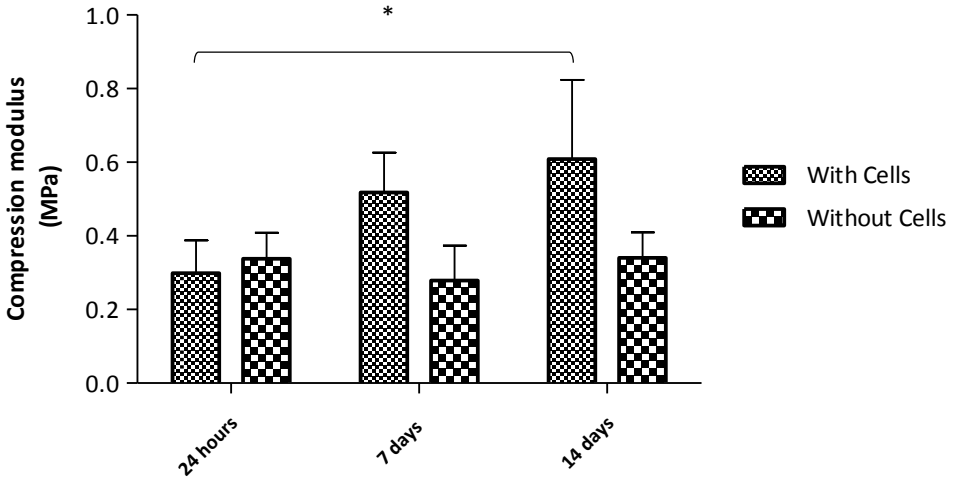

Figure 3:17 Evolution of the value of the compression *modulus* with time of culture for scaffolds with and without cells (control). The error bars correspond to the value of standard derivation of each sample (In terms of statistical relevance *** corresponds to $P < 0.001$;** to $P < 0.01$ and * to $P < 0.05$).

Table 3:7 Compression *moduli* of PTMC scaffolds determined for scaffolds with and without hAFC cells for different culture times. Values are presented with the correspondent value of standard deviation.

	Time of culture (days)	**State of scaffold**	**Compression *modulus* (*MPa*)**
Scaffold without cells	-	Dry	0.210±0.030 [5]
	1	Wet	0.338±0.071
	7		0.279±0.095
	14		0.340±0.069
Scaffold with cells	1	Wet	0.299±0.089
	7		0.518±0.108
	14		0.609±0.215

The results presented in Table 3:7, demonstrate that the wet scaffolds present in average a higher compression *moduli* than the one determined previously for the dry state scaffold [40]. This is contrary to the findings presented by Nadan L. Nerurkar *et al* in 2009 [11] and by Schuller-Ravvo *et al* [22], the latest tested the variation of the compression *moduli* of PTMC scaffolds at different conditions and temperatures, the authors defended that with the uptake of water there is a swelling of the polymer network that leads to a decrease of the compression *moduli*. However the same authors also state that differences between wet and dry scaffolds is less obvious for measurements made at higher temperatures, of about 37 *°C*. This way, and considering that there is no relevant statistical difference between the results obtained for the scaffolds without cells in the different states, it is considered that the minor raise of the compression *moduli* may result from differences between the scaffolds used for the two separated experiments. The results obtained for the compression of the scaffolds 24 hours after seeding are similar to those without cells and only after 7 and 14 days of seeding there is a relevant increase of the value of the compression *moduli* ($P < 0.005$), meaning that for early culture times, maturation of the mechanical properties is not achieved.

With regard to the scaffolds with cells, a growth trend tendency of the value of the compression *moduli* with time was observed, reaching from 0.299±0.089 *MPa* after 24 hours of culture to 0.609±0.215 *MPa* after 14 days of culture. The observed increase is statistically significant, representing a rise of approximately 204 *%* from the initial value ($P < 0.005$; Table 3:7 and Figure 3:17). This is probably due to cell growth and fibrous ECM production, mainly collagen and elastin which raises with culture time. In previous works it was demonstrated that there is an increment of the compression *moduli* value with culture duration, about 50 *%* in 6 weeks [22], for a culture of bovine chondrocytes in PTMC based resins. A similar result was achieved when the mechanical properties of an aligned nanofibrous *poly-Ɛ-caprolactone* seeded with bovine AF cells were tested, proposing that the AF cells produce fibrous ECM that improved the tensile load-bearing capacity of scaffolds and that ECM deposition can improve engineered AF characteristics even when under biaxial deformations [11].

The values of compression *moduli* achieved in the present experiment 0.609±0.215 *MPa* (Table 3:7), fall into the range of the ones reported in the bibliography for human *annulus fibrosus* tissue (0.450-0.800 *MPa*) [8] [40], [41], being greater than the ones obtained by Sebástien Blanquer *et al* [40] for any of the dry PTMC scaffolds without cells, regardless the pore size (230 *μm*,320 *μm* and 420 *μm*). This results change the current believe that smaller pore scaffolds are more suitable for tissue engineering of the AF [40], since they possess bigger compression *modulus* in the dry state, when compared with larger pore sizes [40]. Nonetheless this study proves that 7 to 14 days is enough to mature the mechanical properties of the scaffolds and raise the compression *modulus* of bigger pore size scaffolds, making them suitable for tissue engineering of the AF tissue. Is of utmost importance that the built scaffolds were not too strong and stiff, once generally those kind of constructs have a tendency to produce weak tissues and ECM, which are not able to recover normal tissue functionality, after scaffold degradation.

We consider that the compression *moduli* continues to raise for longer culture times until the scaffold reaches its maximum capacity to held cells, by this time a *plateau* of continuous compression *moduli* value is expected to be formed and it should only decrease when the PTMC material starts to deteriorate. Furthermore according to Schuller Ravoo *et al* in 2011 [39], compression *modulus* values of PTMC porous constructs may increase if the correct mechanical stimuli is applied, reaching 0.450-0.800 *MPa*. For this reason since all PTMC scaffolds used in the current experiment present the same gyroid architecture, a similar growth tendency of the compression *moduli* with culture time is expected for scaffolds with diverse design specifications, if they also present an increase of cell amount.

As expected the control constructs present a constant value of compression *modulus* for the different times. The small variations presented are more likely due to temperature variations between the testing days. As demonstrated before by Schuller-Ravvo *et al* [22], with the raise of temperature from 21 *°C* to 37 *°C* there is a decrease of almost 50 *%* of the compression *moduli* for PTMC-based resins.

Aforesaid, one of the most interesting characteristics of PTMC is its extreme elasticity [39], this characteristic allowed all the PTMC built scaffolds to maintain its shape even after being subjected to high compression forces reached in the compression tests performed. Melchels *et al* demonstrated in 2010 that when gyroid architectures are subjected to compression, stress and strain are homogenously distributed throughout the scaffold [44]. This way is expected that, upon implantation, the cells present in the construct will be equally exposed to the mechanical stimuli in all the structure, which can be beneficial since is known that *annulus fibrosus* cells respond to matrix deformation [44].

During the scaffold's compression there are two different phases that are clearly distinguishable in the stress-strain curves in Figure 3:18. These are intrinsically related with the scaffold's gyroid architecture, being similar to the compression curves previously obtained by Melchels *et al* in 2010, see Figure 7:5 of Annex 7.2.3 [44]. On a first stage, the porous structure is compressed in a way that a gradual abatement of the pores is achieved, which corresponds to a big increase of the strain and a low variation of the applied force. After the collapse of all the pores, an inflection point in the stress-strain curves is formed at about 58 *%* of strain for all constructs, resultant of an increased resistance due to the sole compression of the scaffold's building material,

PTMC. The second stage of compression is characterized by an exponential growth of the applied force needed for the compression of the material.

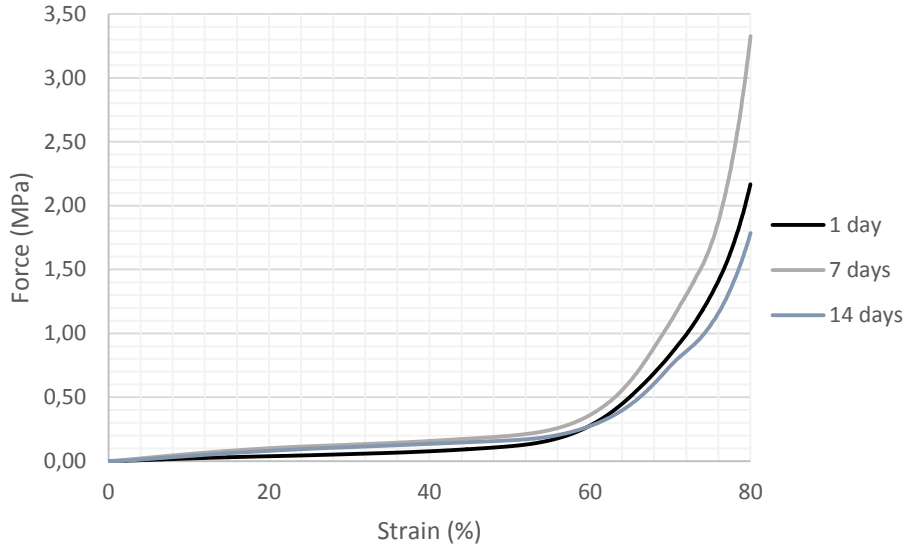

Figure 3:18 Stress-strain curves obtained for PTMC (*Mn* 5000 *g/mol*) scaffolds, variation with time of culture.

Comparing the compression curves obtained for the different time-points, it is possible to detect several alterations that reflect the change of the constructs mechanical characteristics (Figure 3:18). With longer culture times there is a raise in the resistance of the scaffold to compressive forces on the first stage of compression, what is translated in Figure 3:18 in an increase of the inclination of the curve from 0 *%* to 58 *%* strain. More inflection points are also visible in the 7 and 14 days compression curves in both stages of compression, demonstrating that additional resistance to compression arises from cell growth and ECM production.

4. CONCLUSIONS

All the tested scaffolds presented good cell adhesion and proliferation, validating the use of PTMC built scaffolds for tissue engineering of the *annulus fibrosus*. Since hAFC were used, it is expected that after implantation, native cells will have a similar response to the construct, infiltrating and proliferating at similar rates.

Regarding the scaffold design characteristics, it was determined that in terms of cell proliferation and uniform cell distribution, scaffolds with bigger pore sizes (493 μm) and porosities (≥ 67 %) are optimal, most probably allowing proper nutrient diffusion to the inside of the scaffold and removal of toxic metabolites from inside the scaffold formed by cellular normal activity. Also, larger pores will initially provide better cell adhesion [(40)] and less aggregate formation [(57)], comparing to smaller pores. Combination of high porosities and pore sizes, diminishes the space in the construct occupied by the scaffold's material, this way pores are filled with greater amounts of cells and ECM, what facilitates the regeneration process since native cell and ECM densities should be more easily achieved [(57)].

It was also observed that better cell proliferation, was connected to greater values of specific surface area (≥ 7,36 μm^{-1}). Exposition of cells to the surface properties, such as chemical and topographical characteristics of the constructs [(56)], proved to be beneficial. However surface properties of the scaffolds were not analysed in the present research, but should be considered in future testing.

The porous PTMC constructs presented a significant maturation of their mechanical properties, with a trend of increase of over two times their initial value of compression *moduli* after 14 days of static culture (from 0.299±0.089 *MPa* to 0.609±0.215 *MPa*). This is important when it regards implantation, since after a small culture period scaffolds can be implanted, given the necessary mechanical support for cell growth, with no significant difference between the compression *moduli* of the native tissue to that of the graft.

This study proved that scaffolds designed and built with larger pore sizes (400 μm) are a better solution for repair of the AF tissue, compared to smaller pore size scaffolds (≤ 383 μm), since they present better cell distribution and proliferation, having great mechanical performance. This last may reduce the recovery time of surgeries, once biofunctionality is readily achieved.

Overall it was demonstrated that gyroid architecture PTMC scaffolds built using stereolithography hold a great potential for tissue engineering of the *annulus fibrosus* with possible re-establishment of the biomechanical function of the IVD. However further research was to be conducted, regarding *in vivo* testing performance and delivery strategies.

5. FUTURE PERSPECTIVES

Optimization of scaffold's design for application on tissue engineering of the *annulus fibrosus* is extremely hard to achieve, since all design parameters are dependent on each other and small alterations may drastically change cell response and behaviour. We suggest that in a short term, further research should focus on determination of optimal specific surface area and further characterization of the mechanical properties of the constructs, including elastic *modulus* and shear *modulus*.

Furthermore, studies with the already determined optimal conditions, pore size and porosity, should be conducted over longer periods of time, up to 6 months, to assess cell viability, extracellular matrix production, material degradation rates and mechanical properties maturation. Simultaneously, constructs should be dynamically cultured using a bioreactor that mimics the native AF microenvironment, in order to assess the effect of mechanical stimuli on gene expression and ECM production, comparing the results to those of human *annulus fibrosus*.

Additional alterations to the scaffold's design, like application of a controlled pore size gradients [46] (see Annex 7.2.3) should be considered in order to mimic the structural differences between inner and outer AF. Scaffolds with a variation of pore size would be advantageous for repair of larger AF injuries, since controlled gradients were proven to have intermediate mechanical and morphological properties, when compared to homogenous pore size scaffolds [46]. A similar variation of mechanical properties is observed in the different parts of the AF, and by applying a gradient, specific mechanical stimuli would be applied in the different areas maintaining at each zone, the cell's phenotypes. Addiction or combination with different materials could also prove to be beneficial, enabling the delivery of biologics or enhancing the mechanical properties [28] of the constructs.

Overall, further research should include an adequate strategy for graft implantation and fixation *in vivo*, that ensures the functionality and viability of the tissue engineered *annulus fibrosus*.

6. BIBLIOGRAPHIC REFERENCES

1. *Annulus fibrosus tissue engineering using lamellar silk scaffolds.* Park, Sang Hyug, et al. s.l. : Wiley Online Publisher, 2012, Journal of Tissue Engineering and Regenerative Medicine, Vol. 6, pp. 24-33.

2. *Tissue engineering strategies applied in the regeneration of the human intervertebral disk.* Silva-Correia, Joana, et al. 8, 2013, Biotechnology advances, Vol. 31, pp. 1514-31.

3. *Intervertebral disc regeneration or repair with biomaterials and stem cell therapy - feasible or fiction?* Chan, Scw and Gantenbein-Ritter, B. May, s.l. : The European Journal of Medical Sciences , 2012, Swiss Medical Weekly, Vol. 142.

4. S.G.Rotman. *The effect of scaffolds characteristics on the growth of Annulus Fibrosus Cells.* Enschede : Universiteit Twente, 2013.

5. *Acid-Sensing Ion Channels in Healthy and Degenerated Human Intervertebral Disc.* Cuesta, Antonio, et al. 3, s.l. : Informa heathcare, 2014, Connective tissue research, Vol. 55, pp. 197-204.

6. *Translation of an engineered nanofibrous disc-like angly-ply structure for intervertebral disc replacement in a small animal model.* Martin, John T, et al. s.l. : Elsevier, 2014, Acta Biomaterial, Vol. 10, pp. 2473-2481.

7. *Mechanobiology of the intervertebral Disc and Relevance to Disc Degeneration.* Setton, Lori A. and Chen, Jun. 2006, The Journal of Bone and Joint Surgery, Vol. 88, pp. 52-57.

8. *Challenges and strategies in the repair of ruptured annulus fibrosus.* Guterl, C C, et al. s.l. : Ecmjournal.org, 2013, European cells & materials, Vol. 25, pp. 1-21.

9. *Biologic repair and regeneration of the intervertebral disk.* An HS, Masuda K, Cs-Szabo G, Zhang Y, Chee A, Andersson GB, Im HJ, Thonar EJ, Kwon YM. 2011, J Am Acad Orthop Surg, Vol. 19, pp. 450–452.

10. *Repair, Regenerative and supportive theraphies of annulus fibrosus: achievements and challanges.* Bron, Johanes L., Helder, Marco N. and Meisei, Hans-Jorg et all. s.l. : Springer, 2009, European Spine Journal, Vol. 18, pp. 301-313.

11. *ISSLS prize winner: integrating theoretical and experimental methods for functional tissue engineering of the annulus fibrosus.* Nerurkar, Nandan L, Mauck, Robert L and Elliott, Dawn M. 25, s.l. : Lippincott Williams & Wilkins, 2008, Spine, Vol. 33, pp. 2691-2701.

12. *Annulus Fibrosus Cell Characteristics are a Potential Source of Intervertebral Disc Pathologenesis.* Jin, Lin, et al. [ed.] Dominique Heyman. 5, May 2014, Plos One, Vol. 9.

13. *Tissue engineering of annulus fibrosus using electrospun fibrous scaffolds with aligned polycaprolactone fibers.* Koepsell, Laura, et al. 4, 2011, Journal of biomedical materials research. , Vol. 99, pp. 564-75.

14. *Role of biomechanics in intervertebral disc degeneration and regenerative therapies: what needs repairing in the disc and what are promising biomaterials for its repair?* 3, s.l. : Elsevier, 2013, The spine journal : official journal of the North American Spine Society, Vol. 13, pp. 243-62.

15. *Effect of orientation and targeted extracellular matrix degradation on annulus fibrosus shear mechanical properties.* Jacobs, Nathan T., Smith, Lachlan J. and Han, Woojin M. et al. 8, s.l. : Elsevier, 2011, J Mech Behav Biomed Mater, Vol. 4.

16. *Modulation of annulus fibrosus cell alignment and function on oriented nanofibrous polyurethane scaffolds under tension.* Turner, Kathleen G., Ahmed, Nazish and Santerre, J. Paul and Kandel, Rita. 3, s.l. : Elsevier, 2014, Spine Journal, Vol. 14, pp. 424-434.

17. *Optimization of material parameter identification in biomechanics.* Harb, N, Label, N. and Domaszewski, M. and Peyraut, F. s.l. : Springer , 2014, Sturct Multi dusc Optim : Medical and Bioengineering Applications, Vol. 49, pp. 337-349.

18. *The molecular basis of intervertebral disc degeneration.* Kepler, Christopher K, et al. 3, s.l. : Elsevier, 2013, The Spine Journal, Vol. 13, pp. 318-30.

19. Why Herniated Discs Hurt – Causes of Back Pain. *Spinalstenosis.org.* [Online] [Cited: 30 August 2014.] http://spinalstenosis.org/blog/herniated-discs-hurt-pain/.

20. Iatridis, James C. Spine Bioengineering Laboratory . *emba - Researching Intervertebral Disc Mechanobiology.* [Online] [Cited: 31 August 2014.] http://www.emba.uvm.edu/~jiatridi/research/research.html.

21. *The challenge and advancement of annulus fibrosus tissue engineering.* Jin, Li, Shimmer, Adam L and Li, Xudong. 5, s.l. : Springer, 2013, European Spine Journal , Vol. 22, pp. 1090-100.

22. *Flexible and Elastic Scaffolds for Cartilage Tissue Engineering Prepared by Stereolithography Using Poly(trimethylene carbonate)-Based Resins.* Schuller-Ravoo, Sigrid, Feijen, Sandra M. Teixeira. Jan and Grijpma, Dirl W. s.l. : Wiley Online, 2013, Macromolecular Bioscience, Vol. 13, pp. 1711-1719.

23.Evidence-based Medicine*: Discogenic Low Back Pain.* Kallewaard, Jan Willem and Terheggen, Michel A. M. B. T et al. 6, 2010, Pain Practice, Vol. 10, pp. 560-579.

24. *Biological repair of the degenerated intervertebral disc by the injection of growth factors.* Masuda, Koichi. 4, 2008, European Spine Journal, Vol. 17.

25. *Gene therapy for intervertebral disk degeneration.* Woods B, Vo N, Sowa G, Kang JD. 4, s.l. : Elsevier, 2011 , Orthop Clin North Am, Vol. 42.

26. Dr Frank Gaillard . Lumbar disc arthroplasty. *Radiopaedia.org.* [Online] 2008 August 23. [Cited: 11 September 2014.] http://radiopaedia.org/images/6868.

27. *Lumbar Disc Disorders and Low-Back Pain: Socioeconomic Factors and Consequences.* Katz, Jeffrey N. 4, 2006 , J Bone Joint Surg Am, Vol. 88, pp. 21-24.

28. *A review on stereolithography and its applications in biomedical engineering.* Melchels, F. P W and Feijen, Jan: Grijpma, Dirk W. 24, s.l. : Elsevier, 2010, Biomaterials, Vol. 31, pp. 6121-6130.

29. *Recent advances in biological therapies for disc degeneration: tissue engineering of the annulus fibrosus, nucleus pulposus and whole intervertebral discs.* Hudson, Katherine D, et al. 5, s.l. : Elsevier, 2013, Current opinion in biotechnology, Vol. 24, pp. 872-9.

30. *Shape-memory porous alginate scaffolds for regeneration of the annulus fibrosus: Effect of TGF-B3 supplementation and oxygen culture.* Guillaume, Oliver, et al. s.l. : Elsevier, 2014, Acta materialia, Vol. 10, pp. 1985-1995.

31. Likhitpanichkul, M., et al. Fibrin-Genipin adhesive hydrogel for annulus fibrosus repair: performance evaluation with large animal organ culture, in situ Biomechanics, and in vivo degradation tests; *European Cells and Materials.* 2014, Vol. 28, pp. 25-38.

32. *Biodegradable Electrospun Scaffolds for Annulus Fibrosus Tissue Engineering: Effect of Scaffold Structure and Composition on Annulus Fibrosus Cells In Vitro.* Grad, S., et al. S01, s.l. : Tissue Engineering, 2012, Global Spine Journal, Vol. 2, pp. 672-82.

33. *Nanofibrous biologic laminates replicate the form and function of the annulus fibrosus.* Nerurkar, Nandan L., et al. s.l. : Nature, 2009, Nature Materials, Vol. 8, pp. 986-992.

34. *Strategies for replicating anatomical cartilaginous tissue gradient in engineered intervertebral disc.* Bhattacharjee, Maumita, et al. 1, 2014, ACS applied materials & interfaces, Vol. 6, pp. 183-93.

35. *Cells scaffold complex for Intervertebral disc Anulus Fibrosus tissue engineering: In vitro culture and product analysis.* Pan, Yong, et al. 9, 2012, Molecular Biology Reports, Vol. 39, pp. 8581-8594.

36. *Porosity and Cell Preseeding Influence Electrospun Scaffold Maturation and Meniscus Integration In Vitro.* Ionescu, Lara C. and Mauck, Robert L. 3, s.l. : Tissue Engineering:, 2013, Vol. 19.

37. *The potential to improve cell infiltration in composite fiber-aligned electrospun scaffolds by the selective removal of sacrificial fibers.* Baker BM, Gee AO, Metter RB, Nathan AS, Marklein RA, Burdick JA, Mauck RL. 15, s.l. : Elsevier, 2008, Biomaterials, Vol. 29.

38. Samantha C. W. Chan, Jochen Walser, Patrick Ka¨ppeli, Mohammad Javad Shamsollahi,Stephen J. Ferguson, Benjamin Gantenbein-Ritter. Region Specific Response of Intervertebral Disc Cells to Complex Dynamic Loading: An Organ Culture Study Using a Dynamic Torsion-Compression Bioreactor. [ed.] University of Utah, United States of America David Carrier. *PLOS one.* e72489, August 2013, Vol. 8, 8.

39. *Advanced Microestructures based on Poly(trimethylene carbonate):.* Schuller-Ravoo, Sigrid. 2011.

40. *Effect of Pore Characteristics on Mechanical Properties and Annulus Fibrous Cell Seeding and Proliferation in Designed PTMC Tissue Engineering Scaffolds.* Blanquer, Sébastien B.G., et al. s.l. : Wiley-VCH, 2013, Macromol. Symp., pp. 75-81.

41. *Effects of the architecture of tissue engineering scaffolds on cell seeding and culturing.* Melchels, Ferry P W, et al. 11, s.l. : Elsevier, 2010, Acta Biomaterialia, Vol. 6, pp. 4208-4217.

42. *Three-dimensional scaffolds for tissue engineering applications: role of porosity and pore size.* Loh, Qiu Li and Choong, Cleo. 6, s.l. : Mary Ann Liebert, Inc., 20113, Tissue engineering., Vol. 19, pp. 485-502.

43. *Preparation of Flexible and Elastic Poly(trimethylene carbonate) Structures by Stereolithography.* Schuller-ravoo, Sigrid, Feijen, Jan and Grijpma, Dirk W. s.l. : Wiley Online Journal, 2011, Macromolecular Bioscience, Vol. 11, pp. 1662-1671.

44. *Mathematically defined tissue engineering scaffold architectures prepared by stereolithography.* Melchels, Ferry P., Bertoldi, Katia and Gabbrielli, Ruggero et all. s.l. : Elsevier, 2010, Biomaterials , Vol. 31, pp. 6909-6916.

45. Yayue Pan, Yong Chen*, Chi Zhou. Fabrication of Smooth Surfaces based on Mask Projection Stereolithography. *Epstein Department of Industrial and Systems Engineering - University of Southern California, Los Angeles, CA 90089.*

46. *Three-dimensional plotted scaffolds with controlled pore size gradients: Effect of scaffold geometry on mechanical performance and cell seeding efficiency.* Sobral, Jorge M, et al. 3, s.l. : Elsevier, 2011, Acta biomaterialia, Vol. 7, pp. 1009-18.

47. *A poly(d,l-lactide) resin for the preparation of tissue engineering scaffolds by stereolithography.* Melchels, F. P W and Feijen, Jan and Grijpma, Dirk W. 23-24, 2009, Biomaterials, Vol. 30, pp. 3801-3809.

48. The Gyroid Triply Periodic Minimal Surface. [Online] Susquehanna University. [Cited: 30 August 2014.] http://www.susqu.edu/brakke/evolver/examples/periodic/gyroid/gyroid.html.

49. *Infinite Periodic Minimal Surfaces Without Self-intersections.* Schoen, Alen H. s.l. : National Aeronautics and Space Administration, 1970, Electronics Research Center .

50. Wikipedia. [Online] [Cited: 30 August 2014.] http://en.wikipedia.org/wiki/Gyroid.

51. Wikipedia. [Online] [Cited: 30 August 2014.] http://en.wikipedia.org/wiki/Minimal_surface.

52. *Reversine Enhances Generation of Progenitor-like Cells by Dediffeerentiation of Annulus Fibrosus Cells.* Saraiya, Mansi, et al. 4, s.l. : Mary Ann Liebert, Inc, 2010, Tissue Engineering, Vol. 16.

53. *Engineered three-dimensional nanofibrous multi-lamellar structure for annulus fibrosus repair.* Kang, Ran, et al. s.l. : RSCPublishing, 2013, Journal Materials Chemistry B, Vol. 1, pp. 5462-5468.

54. *The effect of mean pore size on cell attachment, proliferation and migration in collagen-glycosaminoglycan scaffolds for bone tissue engineering.* Murphy, Ciara M, Haugh, Matthew G and O'Brien, Fergal J. 3, s.l. : Elsevier, 2010, Biomaterials, Vol. 31, pp. 461-6.

55. *The effect of pore size on cell adhesion in collagen-GAG scaffolds.* O'Brien FJ, Harley BA, Yannas IV, Gibson LJ. 4, s.l. : Elsevier, 2005, Biomaterials, Vol. 26, pp. 433-41.

56. *Effect of pore size on ECM secretion and cell growth in gelatin scaffold for articular cartilage tissue engineering.* Lien, Sio M., Ko, Liang Y. and Huang, Ta J. 2, s.l. : Elsevier, 2009, Acta Biomaterialia, Vol. 5, pp. 670-679.

57. *Polymeric Scaffolds in Tissue Engineering Application: A Review.* Dhandayuthapani, Brahatheeswaran, Yoshida, Yasuhiko and Maekawa, Toru and Kumar, D. Sakthi. ii, s.l. : Hindawi Corporation , 2011, International Journal of Polymer Science, Vol. 2011, pp. 1-19.

58. *Lumbar disc degeneration: correlation with age, sex and spine level in 600 autopsy specimens.* Miller, J.A and Schmatz, C. and Schultz, A. B. 173, s.l. : Phila Pa, 1998, Spine, Vol. 13.

59. *Physical properties of high molecular weight 1,3-trimethylene carbonate and d.l-lactide copolymers.* AP, Pêgo and W., Poot A. A.: Grijpma D. 9, s.l. : Material Medicine , 2003, Journal of Material Sciences, Vol. 14, pp. 767-73.

7. ANNEXES

7.1 CONCEPTS

Aggrecan: cartilage-specific proteoglycan core protein, in part responsible for the withstanding of compression forces in cartilage;

Streptomycin: Bactericidal antibiotic;

Penicillin: Bacterial antibiotic (specially gram negative bacteria staphylococci, streptococci);

Amount of pores: Number of pores that can be counted in a line the lateral side of a scaffold;

Autologous Cells: Cells from the recipient and not a donor, from the same individual's body;

Binding sites: Location on the scaffold (probably correspondent to an adsorbed protein or nucleic acids) to which ligands on the cells may form a chemical bond;

Calcein AM: Used in the current study for fluorescence imaging is a molecular probe used to determine cell viability in most eukaryotic cells. When a cell is still viable the non-fluorescent calcein AM is starts to emit a green-fluorescent light after acetoxymethyl ester hydrolysis by intracellular esterases. (Molecular formula $C_{30}H_{26}N_2O_{13}$);

Cartilage: Tissue composed by ECM (GAGs and proteoglycans) and populated by chondrocytes;

Cell Fixation: Before imaging, samples have to be fixated by application of some kind of fixative. In the current study, for the methylene blue staining the fixative used was paraformaldehyde PFA. When applied to the cells, PFA causes the cross-linking of the proteins, without damaging its structure, allowing the visualization of adherent and proliferated cells;

Cell Passing: After growing in a *in vitro* culture systems cells often become confluent and need to be transferred into new vessels by dilution of the initial culture. This process is named cell passing and every time it is applied to a culture of cells the passage number increases. It is considered that cells with a number of passage of 6 or higher is not adequate for Tissue Engineering studies once cells start to differentiate and lose part of their ability to multiply;

Cell Signalling: signalling cells are responsible for the production of extracellular signalling cells that when released have a specific response on the target cells. The target cells have specific receptors that that recognize the released molecules;

Chondrocytes: Majority of the cells present in cartilage, responsible for maintaining its ECM (collagen and proteoglycans). Produces mainly collagen type II that is recognized on the cell surface by an integrin receptor and anchored by fibronectin;

Compression *modulus*: Similar to the Young's *modulus*, results from the material's compression. Is defined as the ratio of the compressive stress applied to a material compared to the resulting compression effect or strain (Pa);

Connective Tissue: Originated from the mesenchyme, supports, connects, or separates different types of tissues and organs of the body. Is composed mainly by ECM and is composed by a great variety of cell types;

Dedifferentiation: phenomenon in which specialized cells regress to an undifferentiated state reminiscent of that of stem cells;

Differentiation: process in which a cell changes its phenotype, by a change on the set of genes that are expressed, to match that of a defined and specialized cell type;

Electrospinning: Fabrication technique that uses electrical charges to continuously produce micro and nano fibres from a liquid polymer solution;

Ethidium Bromide: Used in the current study for fluorescence imaging is a fluorescence tag that connects to the cell's nucleic acids, mainly to DNA. This dye is for this reason used to assess and recognize dead cells, once upon connection with DNA the molecule emits a red-fluorescent light. (Molecular formula: $C_{21}H_{20}BrN_3$)

Fetal bovine serum (**FBS**): liquid plasma remaining after coagulation, without red blood cells. Common supplement for *in vitro* culture of eukaryotic cells, contains growth and adhesion factors, minerals, trace elements, lipids, hormones, albumin and other molecules from an animal origin.

Fibroblast: Morphologically heterogeneous cell type that synthetises and secretes ECM proteins, GAGs and proteoglycans, most common in the connective tissue. Produces mainly collagen type I that is recognized on the cell surface by an integrin receptor and anchored by fibronectin. Normally this kind of cells only divides if needed.

Freeze-drying (lyophilisation): dehydration process were the sample is frozen and then subjected to low pressures that induce the direct sublimation of the most volatile components (usually water). In terms of tissue engineering this technique is used to produce porous scaffolds: first a polymer is added to an adequate solvent and mixed with water to obtain an emulsion. The emulsion is freeze-dried and the water and solvent are removed as described above.

Glycosaminoglycans polysaccharides sequence, with an amino sugar repeating unit along with a uronic sugar. Because of their polar nature, these molecules are easily hydrated, serving in the body as a lubricant or as a shock absorber.

Growth Factors: Molecules, usually proteins or hormones, capable of increasing cellular growth, proliferation or differentiation though stimulation of the cells.

Hyaline cartilage: Simple structured transparent cartilage present in the surface of joints, composed mainly by collagen II and chondroitin sulphate. It has no nerves and no blood vessels.

Integrins: Cell adhesion molecules (CAMs)

Lumbosacral Radiculopathy (lay term: sciatica): compression or inflammation of a spinal nerve that by it term causes a deep and steady radicular pain. This kind of pain can radiate down to the back of the leg to the calf or foot.

Mesenchymal Stem Cells: Multipotent cells. Can differentiate into osteoblasts, chondrocytes and fibroblasts. Adult mesenchymal stem cells can be isolated from the stroma of the bone marrow.

Notocordial cells: cells derived from the mesoderm that are found on the notochord, the embryo's midline structure predecessor in higher vertebrates to the vertebrae and Nucleus Pulposus, serving as an axial skeleton for the embryo. Its resembles cartilage

Phase Separation: Technique in which a solvent with high vapour pressure and low melting point is added to a polymer solution. This mixture is then separated by addition of water that leads to the formation of a polymer-rich and a polymer-poor phase. The two phases are cooled down to the solvent's melting point and then this is removed by sublimation.

Photo-Crosslinking: Formation of a covalent bond that connects one polymer chain to another or different parts of the same macromolecule, in a photo-induced manner.

Polymer functionalization: Addition of small moieties (functional groups of a molecule) or polymers to a main polymer's surface or interface.

Pore size: Average size of the pores present in a construct.

Progenitor cells: Cells that can be further differentiated in some specific cell types.

Proteoglycans: heavily glycosylated proteins present in the connective tissue, consisting in a core protein with one or more GAG chains, covalently attached. Chains are long, linear and negatively charged under physiological conditions.

Salt-Leaching: Technique in which salt crystals (usually NaCl) are put in a scaffold mold and then covered by a polymer solution that is then hardened. The salt is removed by addition of a solvent that leaches the salt out;

Scaffold's Porosity: Percentage of void spaces in the scaffolds (fraction of void volume over the total volume).

Segmental nerves: Nerves attached to a segment of a spine present in a determined organ;

Spinal Stenosis: Narrowing or stenosis of the spinal canal that causes a restriction to the spinal canal, resulting in a neurological deficit. Symptoms include pain, numbness, paraesthesia, and loss of motor control.

Stem Cells: pluripotent cells capable to differentiate into all mature cell types (from ectoderm, endoderm to mesoderm germ layer cells). These are considered undifferentiated

Strain: ratio between the scaffold's extension and its original length ($\Delta L/L$ – normally expressed as a percentage)

Stress: Applied force per material's area (N/m^2).

7.2 INTRODUCTION COMPLEMENTS

7.2.1 Extracellular Matrix components of the AF and NP

The following tables illustrate some of the known properties of the intervertebral disc and its structures, from ECM to mechanical properties. Nevertheless it is important to mention that these change according to the subject age and general health.

Table 7:1 Differences between Annulus Fibrosus and Nucleus Pulposus (Source: Kepler et al 2013 [3])

Feature	AF	NP
Cell shape	Elongated, fibroblast-like	Rounded, chondrocyte-like
Dominant collagen type	Collagen I	Collagen II
Proteoglycan content	Low (~25%)	High (~70%)
ECM water content	Low	High
Biomechanical role	Tensile force to contain NP	Resists axial compression
Primary form of degradation	Loses structural integrity	Loses proteoglycan and water content

Table 7:2 Extracellular components of the *annulus fibrosus* matrix and phenotypical characteristic of the AF (Source: Guterl *et al* 2013 [2])

Marker Molecule	Characteristics (Method used)	Species
Glycosaminoglycan/ hydroxyproline ratio	Ratio 1:6:1 (biochemical assay)	Human
Elastin	Co-localisation with fibrilin-1 (immunohistochemistry)	Human Bovine
Decorin, Lumican	Decreased in aged (>70 years) AF (Western Blot)	Human
Collagen II/ Collagen I ratio	AF<NP<AC (RT-PCR)	Rabbit
Collagen V	AF>NP=AC (RT-PCR)	Rabbit
Collagen I; Collagen III; Collagen V Cadherin-13; Decorin; Versican v3	NP/AF<0,1 (Microarray)	Rat
Laminin B1; Collagen I; Collagen XIV Aquaporin 1; CD 163; Caveolin 3 Haemoglobin beta	NP<AF (Microarray)	Canine
Tenomodulin; TNFAIP6; FOXF1; FOXF2; Aquaporin 1	AF>NP and AC (Microarray, RT-PCR)	Bovine

7.2.2 *Effect of Growth factors Therapies in IVD Repair*

Factor	Species	Model	Dose	Effect
IGF-1	Rat	Compression model	8 ng/8 µl/disc	Clustering of inner anulus cells (single injection)
GDF-5	Rat	Compression model	8 ng/8 µl disc	Clustering of cells, increase in disc height (single injection)
TGF-β	Rat	Compression model	1.6 ng/8 µl disc	Proliferation of cells (multiple injections)
bFGF	Rat	Compression model	8 ng/8 µl/disc	No response
OP-1	Rabbit	Normal	2 µg/10 µl/disc	Increase in disc height, initial PG content in the NP ↑
OP-1	Rabbit	C-ABC—Co-injection	100 µg/10 µl/disc	Increase in disc height, PG content in the NP
OP-1	Rabbit	Needle puncture	100 µg/10 µl/disc	Increase in disc height, improvement of MRI and histology grading scores, PG content in the NP and AF↑ improvement of MRI and histology grading scores
GDF-5	Rabbit	Needle puncture	1 ng, 100 ng, 1 µg, 100 µg/10 µl/disc	Increase in disc height, improvement of MRI and histology grading scores
OP-1	Rabbit	Needle puncture	100 µg/10 µl/disc	Increase in disc height, viscoelastic properties↑
OP-1	Rabbit	After chemonucleolysis Degeneration by C-ABC—4 week after	100 µg/10 µl/disc	Increase in disc height, PG content in the NP and AF↑
BMP-2	Rabbit	Anular tear (5 × 7 mm)	100 µg/100 µl/disc	More degeneration, vascularity and fibroblasts↑
PRP	Rabbit	Nucleotomy	20 µl PRP + Microsphere/disc or 5 µl PRP + 15 µl PBS	PRP + gelatin hydrogel microspheres Less degeneration, more PG PRP only, no effect

IGF-1 insulin-like growth factor; *GDF-5* growth differentiation factor 5; *TGF-β* transforming growth factor-*β*, *bFGF* basic fibroblast growth factor, *OP-1* osteogenic protein-1; *BMP-2* bone morphogenetic protein-2; *PRP* platelet-rich plasma; *C-ABC* chondroitinase-ABC

Figure 7:1 Recent experiments using growth factors effects for culture of IVD *in vivo* [26].

7.2.3 Gyroid Architecture

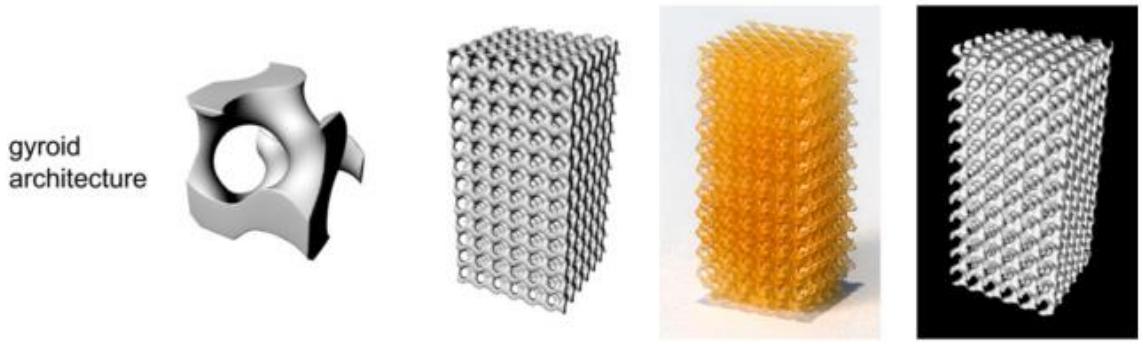

Figure 7:2 Gyroid architecture images. Form the left to the right (CAD-design of a single repeating unit; CAD-design of a entire scaffold construct; Built structure; µCT-scanning of the built structure) (Source: Melchels *et al* 2010) [45]

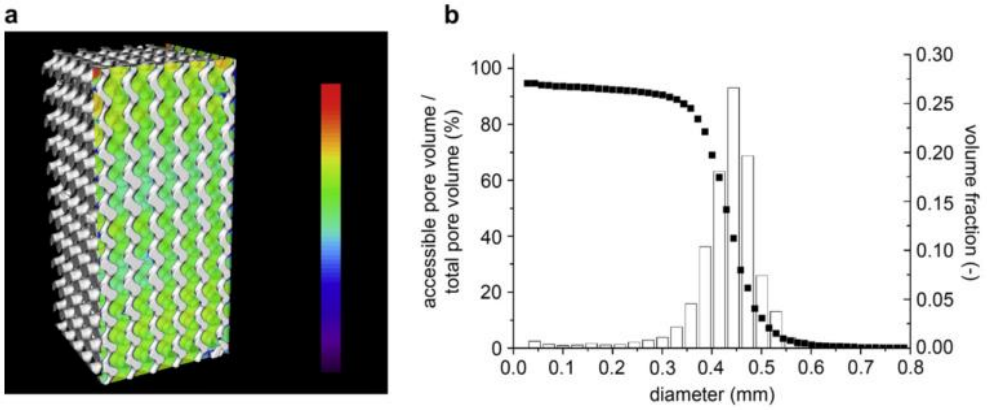

Figure 7:3 Gyroid architecture µCT-scanning image with pore size distribution and accessibility curves of built PDLLA scaffolds (a) Pore size distribution map, each colour corresponds to a pore size (b) Graphic results of µCT-scanning (Source: Melchels *et al* 2010) [45].

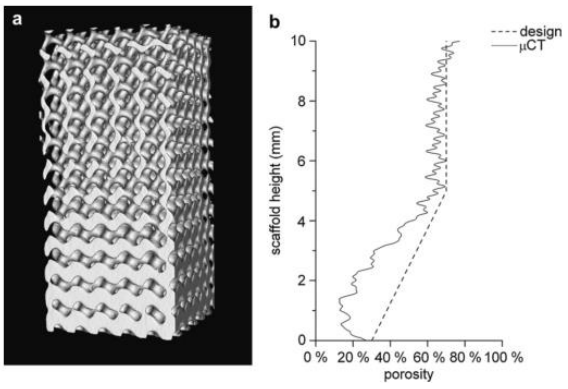

Figure 7:4 Pore sizes gradient scaffold. Variation of pore size with the scaffolds height (Source: Melchels *et al* 2010) [45].

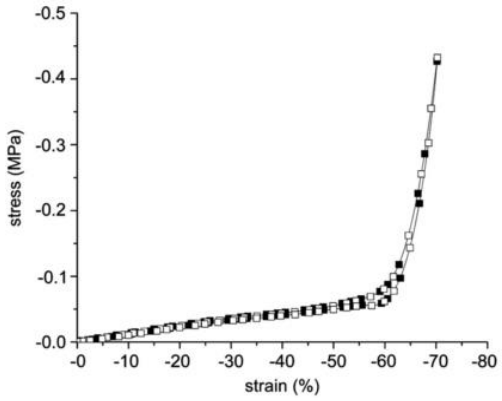

Figure 7:5 Overlay of stress-strain diagrams from cyclic compression (loading-unloading) with strain rate of 30 *%* min^{-1}) of a 69*%* porous P(DLLA-co-CL) gyroid structure (Source: Melchels *et al* 2010) [45].

7.3 METHODS

7.3.1 Cell Culturing and Seeding

Passage 3 hAFCs ($1 \cdot 10^{6}$) previously kept at -120 *°C*, were thawed using a heated water bath at 37 °C and transferred into a 50 *mL* falcon tube filled with 6 *mL* of pre-heated NPCM supplemented medium. The cell suspension was then centrifuged at 300 *CFR* for 5 minutes at room temperature using a Sigma® 6K15 Laboratory Centrifuge. The resultant cell pellet was collected and resuspended in warm medium. About 2 *mL* of cell suspension was added to each T75 flask, in a total of 3 flasks, which contained each about 13 *mL* of supplemented medium.

The total volume of medium was changed every 2 days, until the cells presented approximately 80*%* confluence. To passage the cells the medium was aspirated and the cells washed using DPBS, after which a Trypsin stock solution (0.25 *%*) was applied and the flask incubated for 2 minutes at a 37 *°C* CO_2 incubator, in order to detach the cells from the flask's surface. After incubation 10 mL of medium was added to stop the trypsin action and the solution was centrifuged at 300 *CFR* for 5 minutes, the pallet was recovered, resuspended and the cell suspension was transferred into T175 flasks with 23 *mL* of medium.

For cell seeding, two T175 *mL* flasks were used for each experiment. The medium was aspirated and the content washed with DPBS, then the cells were detached from the flask's surface in a similar manner to that described above. The accurate number of cells were counted using an Automatic Cell Counter from Millipore®, required dilutions to achieve seeding density were performed.

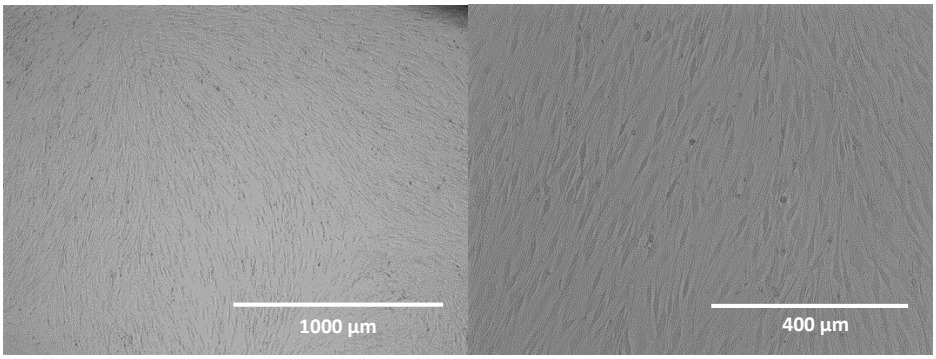

Figure 7:6 Two-dimension growing of human *annulus fibrosus* cells growing in a 175 *mL* T-flask. Passage 4 cells present an elongated shape, similar to that described for native AF cells (Left: *4x* amplification, Right: *10x* amplification).

7.3.2 Cy-Quant® DNA Assay Calibration Curve

To determine the exact cell number at each time of culture a Cy-Quant calibration curve was prepared using a concentrated cell suspension of $1 \cdot 10^6$ passage 4 hAF cells. The cell suspension was centrifuged and the pellet stored at -80 *°C* for a maximum of 4 week. The calibration curve was executed at the day of the sample's reading and the gain for the fluorescence reader was set according to the highest concentration (50 000 cells)

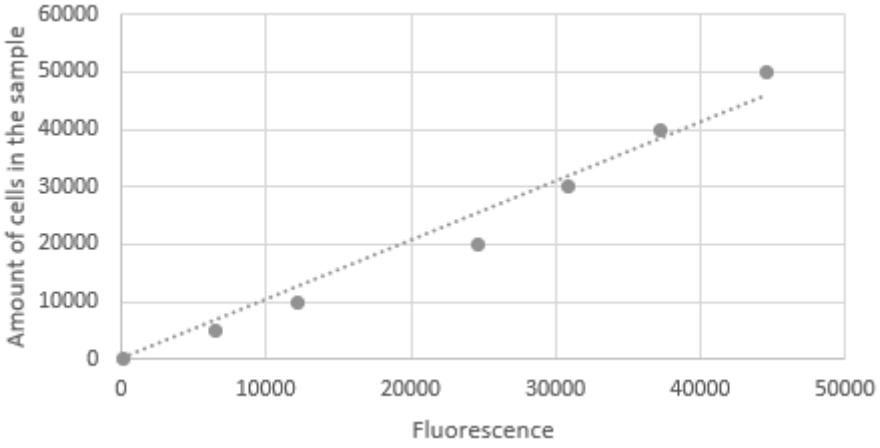

Figure 7:7Calibration curve for determination of cell amount using Cy-Quant® Cell Proliferation assay kit. Calibration executed with passage 4 hAFC cells and using 0.1 *%* Triton X-100 as blank. Obtained calibration curve $\boldsymbol{y = 1,032x}$ with a correlation coefficient R^2= 0.970.

7.4 SUPPLEMENTAL RESULTS

7.4.1 Live/Dead ® Assay

The following pictures are referring to the time of culture of 24 hours and 7 days after seeding. It is possible to see that the cells remain viable with culture time.

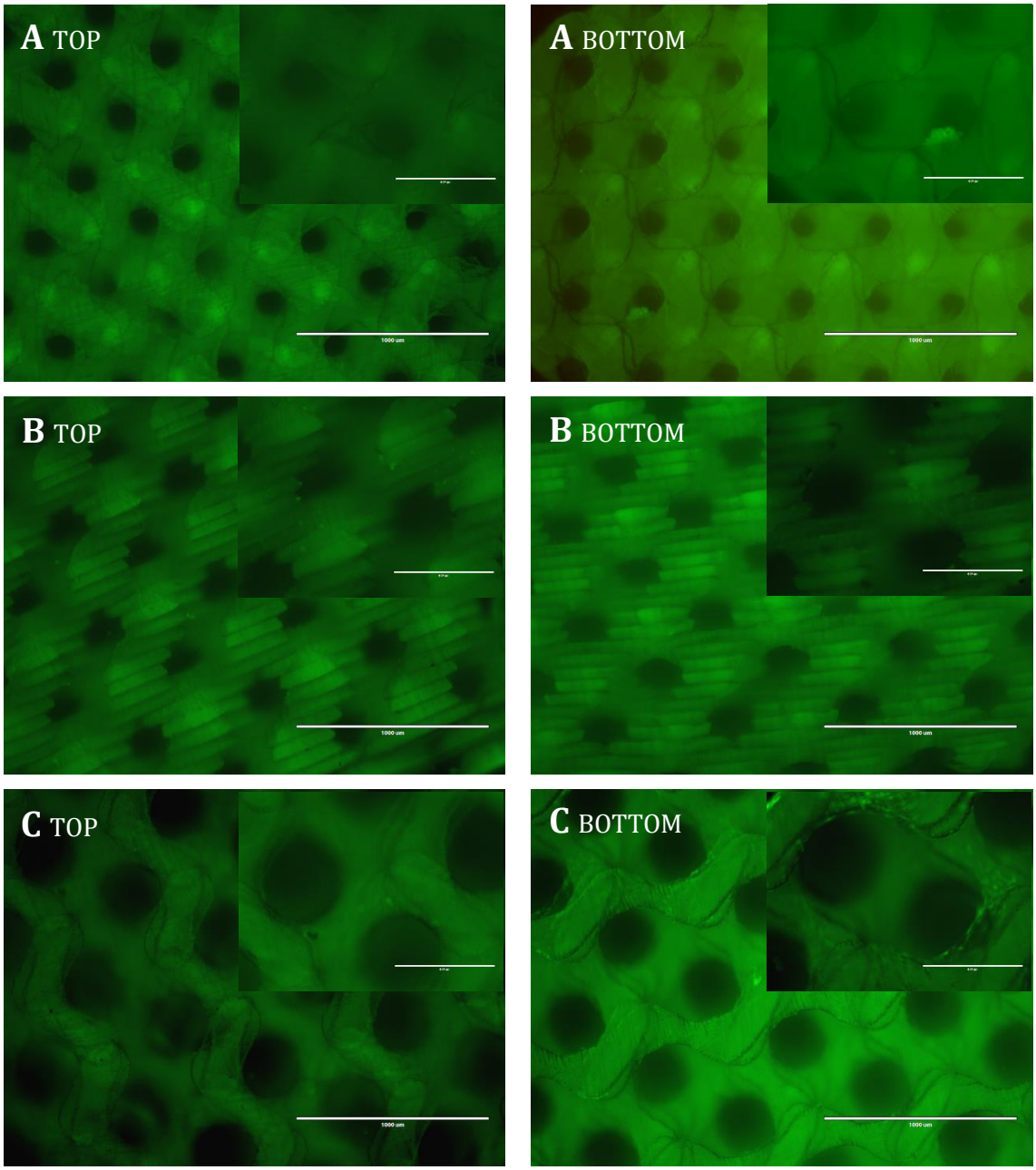

Figure 7:8 Live and Dead® staining of the top and bottom of the scaffolds after 24 hours of culture, detailed view of the cells. Increasing pore size from the top to the bottom (A - 493 μm; B - 383 μm; C - 311 μm).

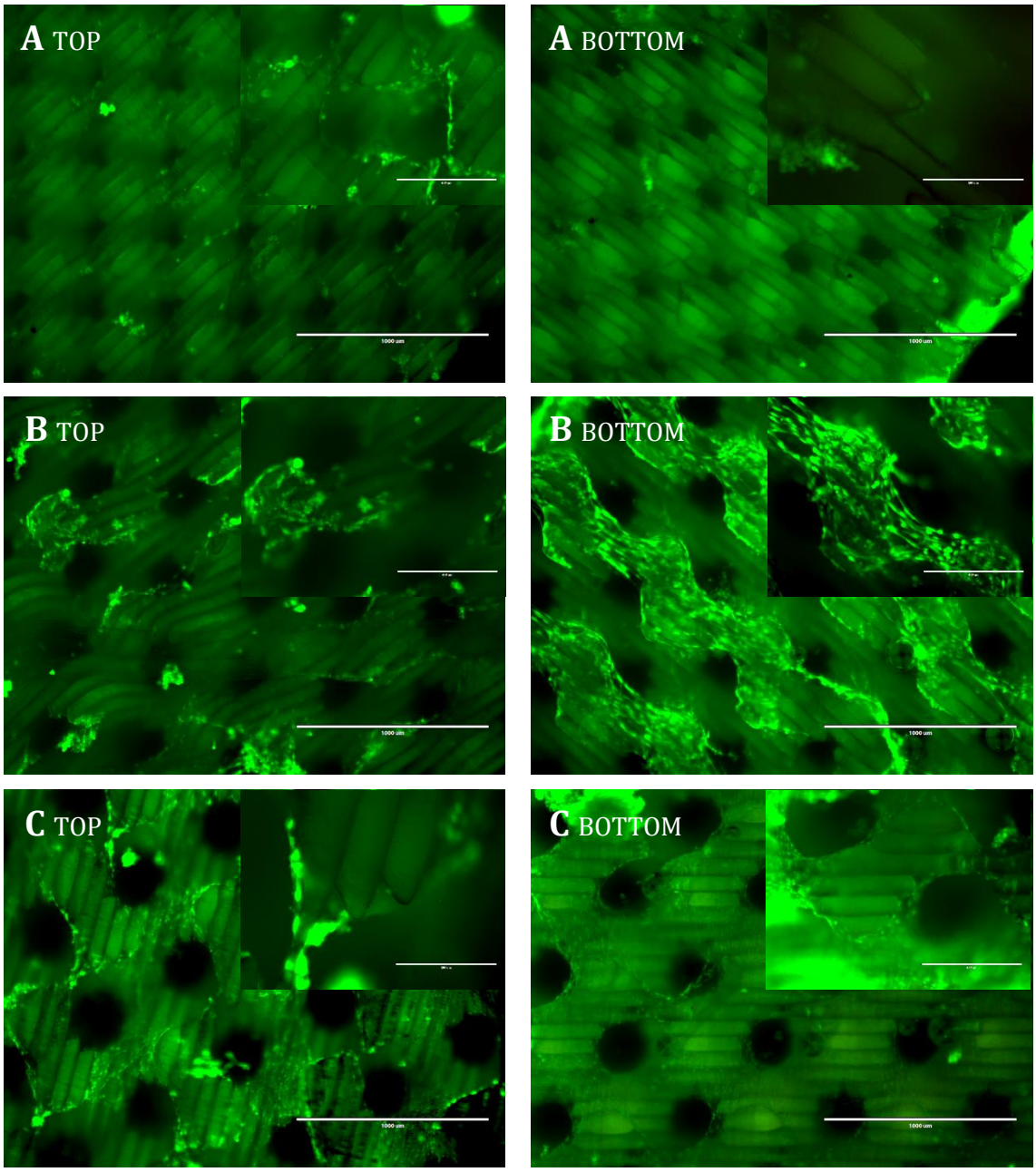

Figure 7:9 Live and Dead® staining of the top and bottom of the scaffolds after 7days of culture, detailed view of the cells. Increasing pore size from the top to the bottom (A - 493 μm; B - 383 μm; C - 311 μm).

7.4.2 Statistical Results

7.4.2.1 Constant Surface Area Experiment

Table 7:3 Statistical results obtained for the experiment of constant specific surface area. Tabular results from GraphPad® Prism 5.

Two-way ANOVA

Source of Variation	% of total variation	P value
Interaction	15,64	< 0.0001
scaffold	15,89	< 0.0001
timepoint	65,31	< 0.0001

Source of Variation	P value summary	Significant?
Interaction	***	Yes
scaffold	***	Yes
timepoint	***	Yes

Bonferroni posttests

62 vs 63

timepoint	62	63	Difference	95% CI of diff.
1 day	1,063	1,000	-0,06311	-0.3264 to 0.2002
7 days	2,669	1,270	-1,399	-1.673 to -1.125
14 days	2,574	2,668	0,09379	-0.1803 to 0.3679

timepoint	Difference	t	P value	Summary
1 day	-0,06311	0,6959	P > 0.05	ns
7 days	-1,399	14,82	P<0.001	***
14 days	0,09379	0,9937	P > 0.05	ns

62 vs 64

timepoint	62	64	Difference	95% CI of diff.
1 day	1,063	1,236	0,1728	-0.09052 to 0.4362
7 days	2,669	3,240	0,5708	0.2725 to 0.8692
14 days	2,574	3,045	0,4706	0.1723 to 0.7689

timepoint	Difference	t	P value	Summary
1 day	0,1728	1,906	P > 0.05	ns
7 days	0,5708	5,556	P<0.001	***
14 days	0,4706	4,581	P<0.001	***

63 vs 64

timepoint	63	64	Difference	95% CI of diff.
1 day	1,000	1,236	0,2359	-0.02741 to 0.4993
7 days	1,270	3,240	1,970	1.681 to 2.258
14 days	2,668	3,045	0,3768	0.08832 to 0.6653

timepoint	Difference	t	P value	Summary
1 day	0,2359	2,602	P < 0.05	*
7 days	1,970	19,83	P<0.001	***
14 days	0,3768	3,793	P<0.01	**

7.4.2.2 Constant Pore Size Experiment

Table 7:4 Statistical results obtained for the experiment of constant pore siza. Tabular results from GraphPad® Prism 5.

Two-way ANOVA

Source of Variation	% of total variation	P value
Interaction	16,87	0,0373
Column Factor	37,80	0,0005
Row Factor	32,91	0,0008

Source of Variation	P value summary	Significant?
Interaction	*	Yes
Column Factor	***	Yes
Row Factor	***	Yes

Bonferroni posttests

57 vs 67

Row Factor	57	67	Difference	95% CI of diff.
1 day	1592	3410	1818	-1424 to 5061
7 days	2608	6201	3593	350.5 to 6835
14 days	1242	4531	3289	46.56 to 6531

Row Factor	Difference	t	P value	Summary
1 day	1818	1,928	P > 0.05	ns
7 days	3593	3,808	P<0.01	**
14 days	3289	3,486	P < 0.05	*

57 vs 77

Row Factor	57	77	Difference	95% CI of diff.
1 day	1592	1071	-521,2	-3763 to 2721
7 days	2608	5699	3090	130.7 to 6050
14 days	1242	5318	4076	1116 to 7035

Row Factor	Difference	t	P value	Summary
1 day	-521,2	0,5525	P > 0.05	ns
7 days	3090	3,589	P < 0.05	*
14 days	4076	4,733	P<0.01	**

67 vs 77

Row Factor	67	77	Difference	95% CI of diff.
1 day	3410	1071	-2340	-5582 to 902.5
7 days	6201	5699	-502,2	-3462 to 2457
14 days	4531	5318	787,2	-2172 to 3747

Row Factor	Difference	t	P value	Summary
1 day	-2340	2,480	P > 0.05	ns
7 days	-502,2	0,5832	P > 0.05	ns
14 days	787,2	0,9141	P > 0.05	ns

7.4.2.3 Mechanical Testing Experiment

Table 7:5 Statistical results obtained for the mechanical tests. Tabular results from GraphPad® Prism 5, Newman-Keuls comparative analysis.

One-way analysis of variance			
P value	0,0175		
P value summary	*		
Are means signif. different? (P < 0.05)	Yes		
Number of groups	4		
F	6,211		
R squared	0,6996		
ANOVA Table	SS	df	MS
Treatment (between columns)	0,3107	3	0,1036
Residual (within columns)	0,1334	8	0,01668
Total	0,4442	11	

Multiple Comparison Test	Mean Diff.	q	Significant? P < 0.05?	Summary
Without cells vs 3rd Time-point	-0,3990	5,351	Yes	*
Without cells vs 2nd Time-Point	-0,3080	4,131	Yes	*
Without cells vs 1st Time-Point	-0,0890	1,194	No	ns
1st Time-Point vs 3rd Time-point	-0,3100	4,158	Yes	*
1st Time-Point vs 2nd Time-Point	-0,2190	2,937	No	ns
2nd Time-Point vs 3rd Time-point	-0,09100	1,220	No	ns